CHALMERS

Calibration of a SONAR Array

Master's Thesis in the Master Degree Programme, Communication Engineering

LIN WEI

Department of Signals and Systems
Division of Communication Engineering
CHALMERS UNIVERSITY OF TECHNOLOGY
Göteborg, Sweden 2012
Master's Thesis EX029/2012

Abstract

Array processing deals with signals received by an array which consists of spatially separated sensors. The purpose of array processing is to extract the interesting signal characteristics by enhancing useful signals and suppressing the noise. Along with the development of digital signal processing techniques, array processing has been an important tool for spatial signal analysis and processing.

As a very important content of array processing, DOA (Direction-of-Arrival) estimation is of great importance in many application areas, and due to this, more and more DOA estimation methods have been proposed over several decades. Generally, these DOA estimation methods rely on several critical assumptions; two of them are listed here: 1) that the response of the sensor array is known in all directions of interest, 2) the spatial covariance of the background noise is known. But neither of them is satisfied in practice, which often results in a serious degradation in algorithm performance [2]. Under this condition, calibration methods are developed to improve the performance of DOA estimation. These methods improve the knowledge of array response, by correcting the modeling errors, such as coupling between sensor elements, mismatch of gain or phase, and direction-dependent perturbations to the sensor response [1]. Thereby, the performance of these DOA estimation methods can be improved by calibration.

This thesis focuses on finding a calibration method to compensate for the non-ideal properties of a specified array, which is the receive transducer unit of multibeam echo sounder system. This array is designed as a uniform linear array with 128 elements and we assume all the elements perform equally. But in practice，due to the deviation of production and components，the elements are not necessarily equally spaced, and they may also have gain/phase shift and mutual coupling. In this thesis, three calibration methods – global diagonal matrix calibration, global full matrix calibration, local calibration- are evaluated to compensate for these non-ideal properties. The implementations of three methods are presented and their performances are also compared. The results show that the local calibration method achieves the best performance and the global calibration methods improve the beamforming in limited DOA range. In addition to this, a brief discussion on frequency dependency of array response is given, and finally a newly developed global calibration method is introduced.

Keywords:

DOA estimation, Beamforming, Mutual coupling, DOA-dependent errors, Global calibration, Local calibration, Calibration with unknown phase and gain.

Acknowledgements / Foreword

This M.Sc thesis has been performed as a collaboration between Chalmers University and Kongsberg Maritime.

I would like to thank my supervisor Mats Viberg for all the help and ideas that he provided. I am grateful for his continuous support, advice and guidance, without which this work would never have been completed.

I would also like to thank all the people at the Department of Signals and Systems, Chalmers University of Technology for their support throughout my Master's studies.

Table of Contents

Terminology / Notation

Abbreviations

DOA	Direction of Arrival
ULA	Uniform Linear Array
UCA	Uniform Circular Array
MUSIC	Multiple Signal Classification
LS-fit	Least-Squares fit

List of Figures

Figure Page

List of Tables

Table Page

Chapter 1 Introduction

Array processing is an important branch of signal processing. A sensor array is composed of multiple spatially separated sensors, used to receive and process the signals. The two most popular geometrical shapes of sensor arrays are ULA (Uniform Linear Array) and UCA (Uniform Circular Array). They are widely used in both military and civilian fields, such as radar, sonar, telecommunication, seismic exploration and medical imaging.

DOA (Direction of Arrival) estimation and Beamforming are the two main concepts in array signal processing. The oldest DOA estimation method, also known as Classical beamforming, used the concepts of spatial match filtering. Later with the development of high-resolution spectrum-based estimation techniques, DOA estimation is distinguished from beamfoming. The goal of DOA estimation techniques is to find a spatial spectrum of the sensor array and calculate the DOAs from this spectrum. They generally take advantage of a precise mathematical model of received array data [1] [6]. Therefore, the resolution and estimation accuracy is limited by noise as well as errors in the assumed data model.

How to improve the performance of DOA estimation when errors exist in the assumed data model has been a hot research topic. In order to correct these errors, many calibration methods have been proposed. Mainly there are two types of methods, one is auto-calibration techniques, which exploit a parametric model of the array response, and include some "array parameters" [1]. The other one is to use sources at known locations. This work focuses on the second type of calibration methods. Three different calibration models with the measured data at known positions are evaluated. The first global diagonal matrix calibration model can only correct the channel errors. The second one, the global full matrix calibration model, can compensate for not only channel errors but also the unknown coupling between array elements [1]. But if there are DOA- dependent errors in the array, the accuracy of DOA estimation cannot be improved significantly by using these two methods. In this case, the third one, local calibration method is proposed. The local calibration method is completely general, but requires more computation and complexity.

The goal of this thesis is to find a suitable calibration method to compensate for the non-ideal properties of the specified array and improve its beamforming. Towards this goal, we set up different calibration models in MATLAB and apply them on the practical measurements. The thesis is organized as follows: Chapter 2 gives a brief introduction to DOA estimation

methods, including the geometric data models and two selected DOA estimation algorithms. Chapter 3 continues with a description of the data model under realistic conditions, and also introduces three error models. Then the corresponding calibration methods are presented in Chapter 4. Chapter 5 shows the experimental processes and gives a comparison of three calibration approaches. Moreover, a frequency dependency analysis of the array response is also included in this section. Chapter 6 gives a further discussion on the calibration method with unknown phase and gain. Concluding comments are placed in Chapter 7.

Chapter 2 DOA Estimation

Estimating the directions of incoming waves from distant sources is a generic problem in array processing. It involves detecting the electromagnetic energy transmitted and captured by antennas or acoustic signals propagated by transducers underwater [1]. Classical beamforming as well as high-resolution DOA estimation methods generally need a prior knowledge of the array response. Thereby, a better knowledge of the array response will provide higher accuracy of DOA estimation. In a purely geometric data model, many real-world factors are not modeled, they are the reasons why the ''real'' array response deviate from the ideal one.

This section introduces the ULA geometric data model including the geometric model of the specified array. Then two selected DOA estimation methods, Classical beamforming and MUSIC (MUltiple Signal Classification), are briefly introduced.

2.1 Geometric data model

The ULA geometry is shown in Figure 1: M sensors of the same type are mounted through a linear array with the same inter-element distance d. Assume the signal comes from the DOA θ. It will be captured by all the elements, but with time delays that depend on the DOAs. Assume there are N time samples available from each sensor. Then, use s(n) and $\mathbf{x}(n)$ to denote the incoming signal vector and array received signal, which is narrowband with center frequency f_c [1] [6].

$$\mathbf{x}(n)=[x_1(n), x_2(n), \dots\dots, x_M(n)]^T, \qquad n=1,2, \dots\dots, N \tag{1}$$

where n=1, 2, ⋯, N denotes discrete time, corresponding to arbitrary continuous-time instances t_n, n=1, 2, ⋯, N.

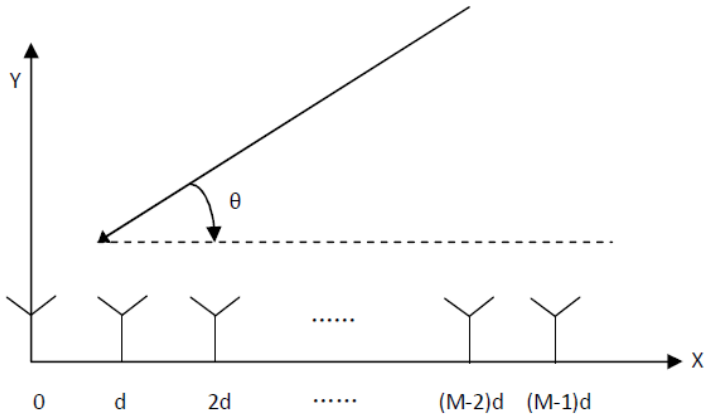

Fig. 1. Uniform Linear Array geometry

According to [1], the ideal sensor array can be modeled by a linear relation as

$$\mathbf{x}(n)= \mathbf{a}(\theta)\, s(n), \tag{2}$$

where $\mathbf{a}(\theta)$ is the array response vector, which takes the form

$$\mathbf{a}(\theta) = g[e^{j2\pi f_c \tau_1(\theta)}, e^{j2\pi f_c \tau_2(\theta)}, \dots\dots, e^{j2\pi f_c \tau_m(\theta)}]^T, \tag{3}$$

Here, g denotes a common gain factor for all elements. It can be g=1 for all elements, or a DOA-dependent gain like g=cos(θ). Further, $\tau_m(\theta)$ denotes the time-delay of a signal at element m, it is a θ-dependent parameter [1]. Assume the signal source is placed in the near field, which means that the incident angle of the signal is different for each element, and the amplitude of the received signal also can be different in each sensor. Here we ignore the amplitude differences and model only the phase response. Using the length between the signal source and a specified element as reference, called L_r; and using L_m to represent the length from the signal source to element m, then the time delay for element m can be calculated as

$$\tau_m(\theta) = [L_m(\theta) - L_r(\theta)]/v, \tag{4}$$

here v is the speed of the signal. Thus, $\mathbf{a}(\theta)$ in (3) can be written as

$$\mathbf{a}(\theta)=g[e^{j2\pi f_c [L_1(\theta)-L_r(\theta)]/v}, e^{j2\pi f_c [L_2(\theta)-L_r(\theta)]/v}, \dots\dots, e^{j2\pi f_c [L_m(\theta)-L_r(\theta)]/v}]^T. \tag{5}$$

Under the assumption of linearity, the superposition principle applies, so the sensor output due to Q near-field emitters can be written as

$$\mathbf{x}(n)=\sum_{q=1}^{Q} \mathbf{a}(\theta_q)\, s_q(n) \; + \; \mathbf{n}(n), \quad n=1,2,\cdots\cdots,N, \tag{6}$$

where θ_q are the DOAs of the signal sources, $s_q(n)$ are the corresponding signal, and $\mathbf{n}(n)$ represents an additive noise term.

Write (6) in compact matrix form, defining the DOA parameters $\boldsymbol{\theta}=[\theta_1, \theta_2, \ldots\ldots, \theta_Q]^T$, array response matrix $\mathbf{A}(\boldsymbol{\theta})=[\mathbf{a}(\theta_1), \mathbf{a}(\theta_2), \ldots\ldots, \mathbf{a}(\theta_Q)]$, and the signal vector $\mathbf{s}(n)=[s_1(n), s_2(n), \ldots\ldots, s_Q(n)]^T$. The resulting model is

$$\mathbf{x}(n)= \mathbf{A}(\boldsymbol{\theta})\mathbf{s}(n) +\mathbf{n}(n), \quad n=1,2,\cdots\cdots,N . \tag{7}$$

If we define $\mathbf{X} = [\mathbf{x}(1), \mathbf{x}(2), \ldots, \mathbf{x}(N)]$, $\mathbf{S} = [\mathbf{s}(1), \mathbf{s}(2), \ldots, \mathbf{s}(N)]$, it can be written more compactly as

$$\mathbf{X}= \mathbf{A}(\boldsymbol{\theta})\mathbf{S} + \mathbf{N}. \tag{8}$$

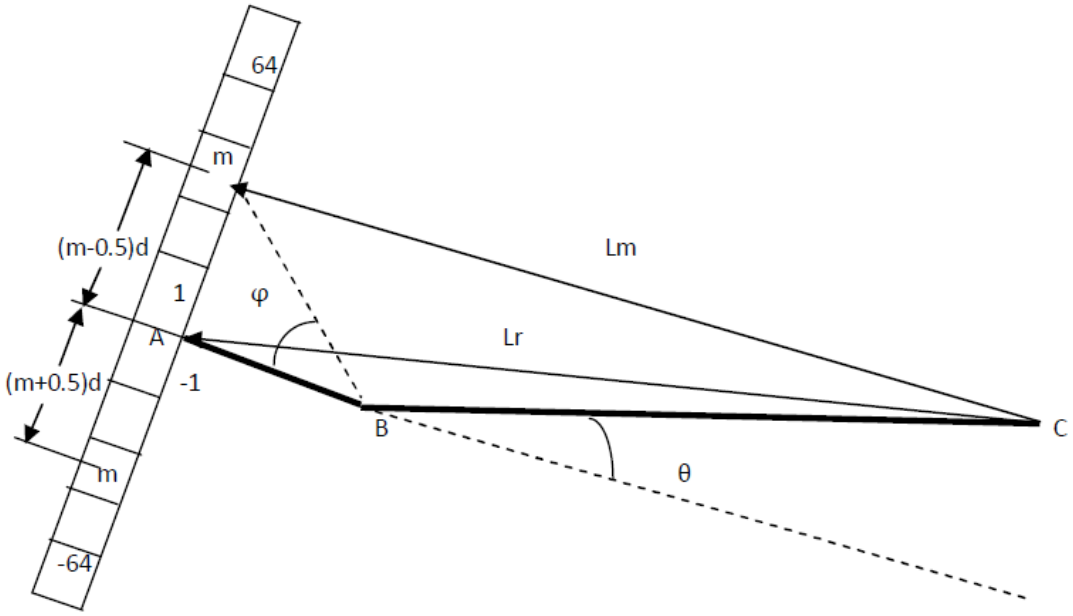

Fig. 2. Measurement Set-up

Figure 2 shows the measurement set-up of the specified array: This array has 128 elements, spaced in a line with the inter-element distance d. Point A is the center of the array, B is the rotation point, and the emitter is fixed at point C. When the array rotates around point B, the direction of arrival θ is changed correspondingly. L_m and L_r can be seen in Figure 2. The reference length L_r is defined as the length from the transducer to the middle, and L_m is the distance from the emitter to each element. The distance between element m and the center of the array is denoted by D. It can be computed as

$$D = (m + 0.5)d \quad \text{for} \quad m < 0$$
$$D = (m - 0.5)d \quad \text{for} \quad m > 0, \tag{9}$$

which can be expressed as:

$$D = [m - \text{sign}(m) \times 0.5]d. \tag{10}$$

The distance between point A and B is a, and the distance between point B and C is b. In order to compute the L_r and L_m, the law of cosines is used, which gives following results:

$$L_r = \sqrt{a^2 + b^2 - 2ab\cos(\pi - \theta)}\ , \tag{11}$$

$$L_m = \sqrt{a^2 + D^2 + b^2 - 2b\sqrt{a^2 + D^2}\ \cos(\pi - \theta - \varphi)}\ , \tag{12}$$

where φ=arctan(D/a).

Assume that all the elements have a DOA-dependent gain, and the gain for each element is approximately equal and given by g=cos(θ). Then, according to (5), the ideal array response vector can be set up as

$$\mathbf{a}(\theta)=\cos(\theta)\ [e^{j2\pi f_c[L_1(\theta)-L_r(\theta)]/v}, e^{j2\pi f_c[L_2(\theta)-L_r(\theta)]/v}, \ldots\ldots, e^{j2\pi f_c[L_m(\theta)-L_r(\theta)]/v}]^T. \tag{13}$$

The ideal array response matrix $\mathbf{A}(\boldsymbol{\theta})$ for DOA parameters $\boldsymbol{\theta}=[\theta_1, \theta_2, \ldots\ldots, \theta_Q]^T$ is expressed as

$$\mathbf{A}(\boldsymbol{\theta})=[\ \mathbf{a}(\theta_1), \mathbf{a}(\theta_2), \ldots\ldots,\ \mathbf{a}(\theta_Q)]. \tag{14}$$

2.2 DOA estimation methods

DOA estimation methods exploit either the parametric structure of the array response or properties of the signals. With the knowledge of ideal array response vector $\mathbf{a}(\theta)$, the directions of incoming signals can be determined by applying the DOA estimation methods on the given observations $\mathbf{x}(n)$.

Equation (7) expresses the sensor output when there are Q signals incident on the M-element array. Assume the covariance Matrix of the white noise vector $\mathbf{N} = [\mathbf{n}(1)\ \mathbf{n}(2)\ \cdots\cdots\ \mathbf{n}(N)]$ is $\sigma^2\mathbf{I}$. Then the array covariance matrix can be written as

$$\mathbf{R_{xx}} = E[\mathbf{x}(n)\mathbf{x}^*(n)] = \mathbf{A}(\boldsymbol{\theta})R_{ss}\mathbf{A}^*(\boldsymbol{\theta}) + \sigma^2\mathbf{I},\ n=1,2,\ldots\ldots,N\ , \tag{15}$$

where $\mathbf{R_{ss}} = E[\mathbf{s}(n)\mathbf{s}^*(n)]$ is the signal covariance matrix. We use $\widehat{\mathbf{R}}_{\mathbf{xx}}$ to denote the estimated array covariance matrix, based on the available measurements, given by

$$\widehat{\mathbf{R}}_{xx} = \frac{1}{N}\sum_{n=1}^{N}\mathbf{x}(n)\mathbf{x}^*(n) = \frac{1}{N}\mathbf{X}\mathbf{X}^*. \tag{16}$$

2.2.1 Classical beamforming

The Classical Beamforming method estimates the DOAs by using a spatially matched filter, which is to coherently combine all sensor outputs as $\mathbf{a}^*(\theta)\mathbf{x}(n)$, then measure the average power. It is computed as follows:

$$\begin{aligned}\mathbf{P}_{BF}(\theta) &= \frac{1}{N}\sum_{n=1}^{N}|\mathbf{a}^*(\theta)\mathbf{x}(n)|^2 \\ &= \mathbf{a}^*(\theta)\left[\frac{1}{N}\sum_{t=1}^{N}\mathbf{x}(n)\mathbf{x}^*(n)\right]\mathbf{a}(\theta) \\ &= \mathbf{a}^*(\theta)\widehat{\mathbf{R}}_{\mathbf{xx}}\,\mathbf{a}(\theta)\ .\end{aligned} \tag{17}$$

The Q DOA estimates can be obtained by finding the Q highest peaks of the spectrum $\mathbf{P}_{BF}(\theta)$.

2.2.2 MUSIC algorithm

In most practical methods, DOA estimation is done by multiplying a weight matrix by the received data matrix. The output power is then calculated. Searching for maximum output power as a function of direction, then gives

the DOA estimates [1] [5].

The MUSIC algorithm is a high resolution subspace-based technique that exploits the eigen structure of the input covariance matrix. In practice, the eigenvectors of $\widehat{\mathbf{R}}_{\mathbf{xx}}$ are separated into two orthogonal subspaces as in equation (18). They are the principle eigen subspace and the non-principle eigen subspace, also named as signal subspace and noise subspace. The dimension of the signal subspace is Q, while the dimension of the noise subspace is M-Q. Their relation can be expressed as

$$\widehat{\mathbf{R}}_{\mathbf{xx}} = \sum_{k=1}^{M} \hat{\lambda}_k \hat{\mathbf{e}}_k \hat{\mathbf{e}}_k^* = \hat{\mathbf{E}}_s \widehat{\mathbf{\Lambda}}_s \hat{\mathbf{E}}_s^* + \hat{\mathbf{E}}_n \widehat{\mathbf{\Lambda}}_n \hat{\mathbf{E}}_n^* \quad , \tag{18}$$

where $\hat{\mathbf{E}}_s$ is the signal subspace, containing the signal eigenvectors $\hat{\mathbf{e}}_k$, $k=1,\cdots,Q$. The noise subspace contains the M-Q smallest eigenvectors of $\widehat{\mathbf{R}}_{xx}$, it is formed as $\hat{\mathbf{E}}_n$. The DOAs $\boldsymbol{\theta}=[\theta_1, \theta_2, \ldots\ldots, \theta_Q]^T$ can be determined by searching through all possible array steering vectors to find those which are orthogonal to the noise subspace. It takes the form

$$\mathbf{P}_{MU}(\theta) = \frac{1}{\mathbf{a}^*(\theta)\hat{\mathbf{E}}_n\hat{\mathbf{E}}_n^*\mathbf{a}(\theta)} \ . \tag{19}$$

The resolution of MUSIC is very high when N and the SNR are sufficiently high. The algorithm fails if the incoming signals are highly correlated [1] [5]. The reason is that in this case the dimension of the signal subspace degrades to some Q', $Q' < Q$. Thus, the noise subspace is "too large", and its corresponding eigenvectors are not all orthogonal to $\mathbf{a}(\theta_q)$, $q=1,\cdots,Q$. Therefore, (19) does not exhibit high peaks near the true DOAs, as is the case for uncorrelated signals.

Chapter 3 Model Errors

As introduced in Chapter 2, the array response $\mathbf{A}(\boldsymbol{\theta})$ used in these DOA estimation methods is obtained from the geometric data model. Those non-ideal properties, without taking into consideration, will inevitably corrupt the performances of DOA estimation methods. For example, the sensor has its own characteristics, determined by the sensor type or the inter-distance between elements, etc. The presence of each element affects the wave-field, this leads to mutual coupling [1][6]. If it is not correctly accounted for, the estimation performance will be influenced significantly.
Besides mutual coupling, some other sources of array modeling errors are :

- Uncertain element positions or orientations.
- Channel imbalance, leading to gain and phase errors at the different sensors.
- Imbalances between the I and Q channels.
- Near-field scattering due to platform or terrain.
- Non-linearity in amplifier, A/D converters, modulators and other hardware.

It is common to model these unknown errors using a so-called correction matrix $\mathbf{Q}$, which modifies the steering vectors from the ideal $\mathbf{a}(\theta)$ to $\mathbf{Q}\mathbf{a}(\theta)$.

The error models used here are the following:

1) $\mathbf{a}_{\text{real}} = \mathbf{Q}_{\text{diag}}\mathbf{a}(\theta)$,

2) $\mathbf{a}_{\text{real}} = \mathbf{Q}\mathbf{a}(\theta)$,

3) $\mathbf{a}_{\text{real}} = \mathbf{Q}_{\text{diag}}(\theta)\mathbf{a}(\theta)$.

where $\mathbf{Q}_{\text{diag}}$ is diagonal matrix, whereas $\mathbf{Q}$ is generally a full matrix.

One common thing in Model 1) and Model 2) is that the correction matrix $\mathbf{Q}$ is direction independent. But in Model 1), the global diagonal matrix, can only correct for channel imbalance. Model 2), the global full matrix, can correct for mutual coupling and channel imbalance. The correction matrix $\mathbf{Q}_{\text{diag}}(\theta)$ in Model 3) is direction dependent, which is completely general and requires the additional assumption that $\mathbf{Q}_{\text{diag}}(\theta)$ is a smooth function of θ to be useful.

Chapter 4 Array Calibration

To remedy these model errors, many calibration methods have been proposed. Reference [1] presents auto-calibration techniques and calibration methods using sources at known positions. In the auto-calibration approach, all parameters are estimated simultaneously, but it requires a parametric model with known structure and relatively few parameters, which is not always satisfied in practice. The second type of calibration methods, with the help of calibration sources at known locations, is a useful remedy. The calibration data is collected by placing a single emitter at several known places, and then it is used to compute the array response vectors for the different source directions [1].

Section 4.1 describes two different ways to estimate the array response vector using the available measurements. With the estimated ''real'' array response, three calibration methods, corresponding to the three error models stated in chapter 3, are introduced in section 4.2.

4.1 Estimation of the ''real'' array response vector

Assume the emitter is placed at known positions θ_c, c=1,……, C, where C is the number of emitter positions, and use N_c to denote the number of data samples taken at position c. Then the calibration data for a signal coming from θ_c can be modeled by

$$\mathbf{x_c}(n)= \mathbf{a_c}s_c(n) +\mathbf{n_c}(n) \text{ , } n=1,2,\cdots\cdots,N_c; \quad c=1,\cdots\cdots, C, \tag{20}$$

where $\mathbf{a_c}=\mathbf{a_c}(\theta_c)$ is the "real" array response vector at θ_c.

The array response vector $\hat{\mathbf{a}}_\mathbf{c}$ can be estimated in two ways, depending on if the incoming signal $s_c(n)$ is known or not. If $s_c(n)$ is known, it can be used to compute $\hat{\mathbf{a}}_\mathbf{c}$ in coherent calibration. If it is unknown, we can use non-coherent calibration to estimate $\hat{\mathbf{a}}_\mathbf{c}$.

4.1.1 Coherent calibration

In this case, $s_c(n)$ is known, the array response vectors can be estimated as

$$\hat{\mathbf{a}}_\mathbf{c}=\frac{\sum_{n=1}^{N_c}\mathbf{x_c}(n)s_c^*(n)}{\sum_{n=1}^{N_c}|s_c(n)|^2} \text{ , } \quad n=1, 2, \cdots\cdots, N_c; \quad c=1,\cdots\cdots, C, \tag{21}$$

In our case, the continuous-time pulse s_c (t) transmitted by the hydrophone under water is described as

$$s_c(t) = \cos(2\pi f_c t + \varphi), \ 0 \le t < T, \tag{22}$$

where T is the observation time, f_c is the frequency and φ is the phase. One thing needed to be pointed out is that the amplitude and phase of $s_c(t)$ are unknown. Thus, we assume its amplitude is 1 and the phase φ is equal to 0°. With this information, the sampled signal $s_c(n)$ can be simulated in MATLAB.

4.1.2 Non-coherent calibration

When s_c is unknown, the array response is computed from the principal eigenvector of the covariance matrix

$$\widehat{\mathbf{R}}_{\mathbf{c}} = \frac{1}{Nc}\sum_{n=1}^{Nc} \mathbf{x_c}(n)\mathbf{x_c^*}(n) = \sum_{k=1}^{M} \hat{\mathbf{e}}_{\mathbf{k}}\hat{\mathbf{e}}_{\mathbf{k}}^{*} \rightarrow \hat{\mathbf{a}}_{\mathbf{c}} \propto \hat{\mathbf{e}}_{\mathbf{1}}. \tag{23}$$

In this case, the resulting estimates have a gain and phase ambiguity, and need to be normalized before the calibration vectors are used [1].

4.2 Calibration methods

As introduced in Chapter 3, we use $\mathbf{Q}$ to modify the ideal array response vector $\mathbf{a}(\theta_c)$ to the "real" array response vector $\hat{\mathbf{a}}_\mathbf{c}(\theta_c)$, which can be formed as

$$\hat{\mathbf{a}}_\mathbf{c}(\theta_c) = \mathbf{Q}\mathbf{a}(\theta_c). \tag{24}$$

If $\mathbf{Q}$ is a calibration matrix which is unchanged for all DOAs, like in error model 1) and 2), then these models are called global calibration model; if $\mathbf{Q}$ is a DOA-dependent correction matrix like in error model 3), then it is a local calibration model.

For both global and local calibration, the correction matrix is determined by using a least-squares fit (LS-fit). This is written as

$$\widehat{\mathbf{Q}} = \arg\min_{\mathbf{Q}} \left\| \hat{\mathbf{A}}_\mathbf{c} - \mathbf{Q}\mathbf{A}(\theta_\mathbf{c}) \right\|^2, \tag{25}$$

where $\mathbf{A}(\theta_\mathbf{c}) = [\mathbf{a}(\theta_1), \dots, \mathbf{a}(\theta_C)]$ is the ideal steering vectors at calibration locations, and $\hat{\mathbf{A}}_\mathbf{c} = [\hat{\mathbf{a}}_1, \dots, \hat{\mathbf{a}}_C]$ is the estimated array response using either (21) or (23).

4.2.1 Global calibration methods

1) If $\mathbf{Q}$ is a diagonal matrix, which can correct for channel errors only. In this case, $\mathbf{Q}$=diag{$\mathbf{q}$}, the elements of $\mathbf{q} = [q_1, \dots\dots, q_M]^T$ are estimated by solving from (25) as

$$\hat{q}_m = \hat{\mathbf{A}}_{c,m}\mathbf{A}_m^*(\theta_c)(\mathbf{A}_m(\theta_c)\mathbf{A}_m^*(\theta_c))^{-1}, \tag{26}$$

where $\hat{\mathbf{A}}_{c,m}$ is the mth row of the estimated "real" array response matrix, and $\mathbf{A}_m(\theta_c)$ is the mth row of the ideal array response matrix.

2) If $\mathbf{Q}$ is a full matrix, this model can correct not only channel errors but also mutual coupling, and the solution for (25) is now

$$\widehat{\mathbf{Q}} = \hat{\mathbf{A}}_\mathbf{c}\mathbf{A}^*(\theta_c)(\mathbf{A}(\theta_c)\mathbf{A}^*(\theta_c))^{-1}. \tag{27}$$

Here, $C \geq M$ is necessary to guarantee a unique solution.

4.2.2 Local calibration methods

3) Global calibration methods are simple and efficient, but they cannot handle DOA-dependent errors, for example due to uncertain element positions. Local calibration methods are developed to solve this drawback; its correction matrix is DOA-dependent and can be expressed as

$$\hat{\mathbf{a}}_{\mathbf{c}} = \mathbf{Q}(\theta_c)\mathbf{a}(\theta_c), \tag{28}$$

where $\mathbf{Q}(\theta_c)$=diag{$\mathbf{q}(\theta_c)$}, and $\mathbf{q}(\theta_c)$ is computed as

$$\hat{\mathbf{q}}(\theta_c) = \hat{\mathbf{a}}_{\mathbf{c}}./\mathbf{a}(\theta_c), \tag{29}$$

here ./ denotes element-wise division. The correction matrix is computed as a function of θ_c. By doing interpolation in the real and imaginary parts of $\hat{\mathbf{q}}(\theta_c)$, $\hat{\mathbf{q}}(\theta)$ at a certain desired DOA θ can be obtained.

Compared to the global calibration, local calibration is more complicated, but its ability of handling general model errors gives a great improvement on DOA estimation performance under severe modeling errors.

Chapter 5 Experimental Results and Analysis

The available measurements are obtained on the specific sensor array underwater, which is a uniform linear array with M=128 elements. The geometrical structure of the emitter and the array is described in Figure 2. Measurements are made for $-100^{\circ} \leq \theta_c \leq 100^{\circ}$. The number of emitter positions C could not be fixed for each measurement, it is a number between 230 and 270. Also the calibration positions $\boldsymbol{\theta_c} = [\theta_1, \ldots\ldots, \theta_c]$ are not exactly the same for each measurement, but the angle difference between any two neighboring positions is around 0.7 degrees, which can be expressed as $\theta_{c+1} - \theta_c \approx 0.7^{\circ}$.

For each emitter position θ_c, the output of the array defined is as $\mathbf{x}(\theta_c)$. It is a M×Nc matrix, where M=128 is the number of elements and Nc=100 is the number of data samples taken at position c. When the array rotates from -100° to 100°, the received data $\mathbf{x}(\theta_c)$ can be regarded as a function of the DOA θ_c. The full data set is thus a three dimensional object expressed as a M×Nc×C tensor.

Since the receiver array operates on frequencies ranging from 200 KHz to 400 KHz, measurements are collected from 160 KHz to 450 KHz at intervals of 10 KHz. One dataset contains 30 data bins covering the 30 different carrier frequencies, and each data bin contains a M×Nc×C matrix. Each new produced array has its own number, so the datasets are named after the tested array. For example, dataset 112 means the measurements are done on the array number 112; and datasets 124_1, 124_2 and 124_3 mean that these measurements are done on the very same arrays.

For an easier presentation, the carrier frequency f_c is first fixed to 250 KHz, and dataset 112 is chosen to explain how to obtain the ideal and ''real'' array response from Sections 5.1 and 5.2. Sections 5.3 and 5.4 also use the same dataset and frequency to show the implementation of the global and local calibration methods. So if there is no special notation, the figures in these four sections are obtained by using dataset 112 and f_c=250 KHz.

In order to compare the calibration performance overall and observe the frequency dependency of the array response, Sections 5.5 and 5.6 use different datasets and change frequencies from 200 KHz to 400 KHz. The used dataset and frequency are stated in the respective figure/table caption.

5.1 Ideal array response A

Section 2.1 describes how we set up the ideal array response model according to the geometric model. It is expressed in the following equations.

$$\mathbf{a}(\theta)=\cos(\theta)\ [e^{j2\pi f_c[L_1(\theta)-L_r(\theta)]/v}, e^{j2\pi f_c[L_2(\theta)-L_r(\theta)]/v}, \dots\dots, e^{j2\pi f_c[L_m(\theta)-L_r(\theta)]/v}]^T, \quad (30)$$

$$\mathbf{A(\theta)} =[\ \mathbf{a}(\theta_1), \mathbf{a}(\theta_2), \dots\dots,\ \ \mathbf{a}(\theta_Q)],\ \ \boldsymbol{\theta}=[\theta_1, \theta_2, \dots\dots, \theta_Q]^T. \quad (31)$$

Here, f_c is fixed to 250 KHz and the underwater speed of sound v is 1481 m/s. Since the useful DOA range in our case is [-80 80] degree, we use a little larger DOA range [-85 85] degree to generate the ideal array response.

Figures 3 and 4 plot the gain and phase of the ideal array response **A(θ)** respectively. In Figure 3, the gain is cosine shaped g = cos(θ) as assumed in the geometric data model. It is DOA-dependent and has the same gain for all elements for a selected DOA. The phase in figure 4 is smooth and continuous, but for the elements at the edge, like element 1 and element 128, their phases have larger variations. The phases of the elements in the middle vary gently. That is because the ideal phase of element m is $2\pi f_c[L_m(\theta) - L_r(\theta)]/v$, it relies on the distance between the emitter and element m, $L_m(\theta)$. For the middle elements, L_m varies slightly versus the DOA θ.

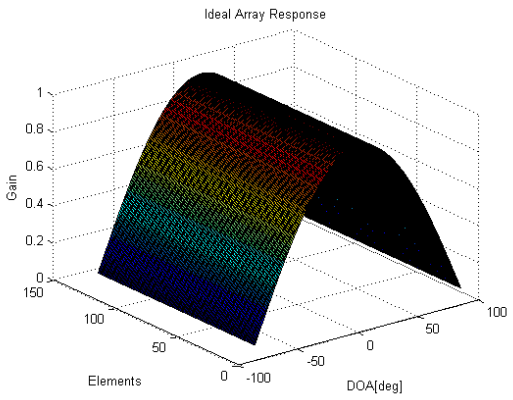

Fig. 3. Gain of the ideal array response f_c=250 KHz, DOA=[-85, 85] deg

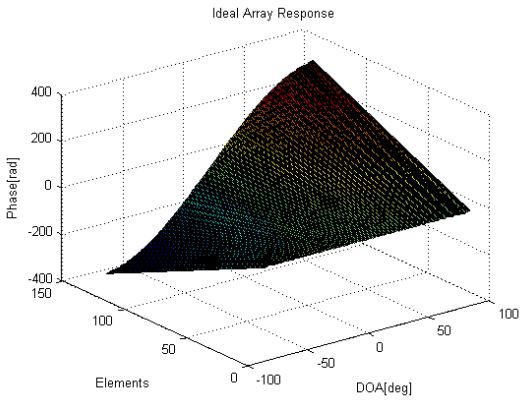

Fig. 4. Phase of the ideal array response f_c=250 KHz, DOA=[-85, 85] deg

5.2 Estimated array response

With the measurements at known positions, the "real" array response can be estimated. Sections 4.1.1 and 4.1.2 describe two methods to obtain the estimated array response. One is coherent calibration, which needs the information of transmitted signal. The transmitted signal $s_c[n]$ is generated in MATLAB under the assumptions of amplitude 1 and phase 0°. In practice, that means that $s_c[n]$ has unknown gain and phase. This may result in a fact that coherent calibration could not get a better estimation than the second method, non-coherent calibration. In non-coherent calibration, the estimated array response is computed from the principal eigenvector of the covariance matrix, without using $s_c[n]$.

By applying these two calibration methods on the measured data $\mathbf{x}(\theta_c)$, the "real" array response $\widehat{\mathbf{A}}_c$ can be estimated and it is shown in the following figures. Figures 5, 6, 7 and 8 show the estimated results from the coherent calibration and non-coherent calibration methods respectively. The results are almost the same, which may be due to the unknown phase and gain. In section 6, we will have a further discussion on calibration methods with unknown phase and gain.

Figures 5 and 7 show the gain of the estimated "real" array response vector, which is not as smooth as the ideal array response gain g=cos(θ). It can be explained by elements position deviations and mutual coupling in the practical environment.

Figure 6 and 8 show the phase of the estimated array response, which looks different from Figure 4 - the phase of the ideal array response, especially for the elements in the middle, their performances are quite different. In order to observe it clearly, Figure 9 plots the phase of element 64. The estimated array response phase does not have the similar behavior as the ideal model. It's easy to observe that there is a turning point around the DOA = 10 degree, which may be due to mutual coupling and phase shifting.

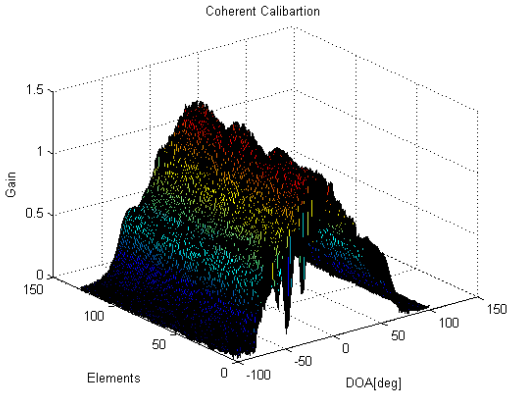

Fig. 5. Coherent calibration
Amplitude of the estimated array response
f_c=250KHz, DOA=[-100, 100] deg

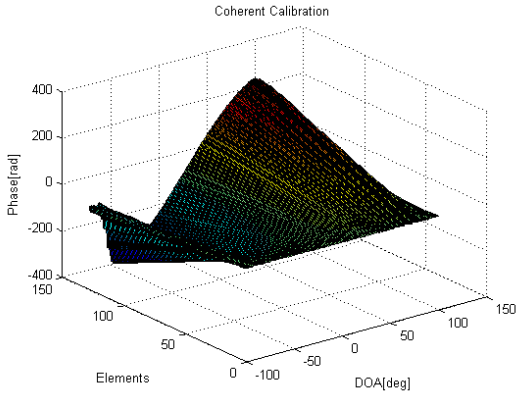

Fig. 6. Coherent calibration
Phase of the estimated array response
f_c=250KHz, DOA=[-100, 100]

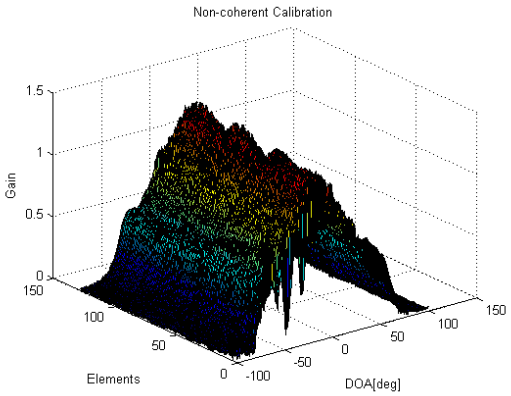

Fig. 7. Non-coherent calibration
Amplitude of the estimated array response
f_c=250KHz, DOA=[-100, 100] deg

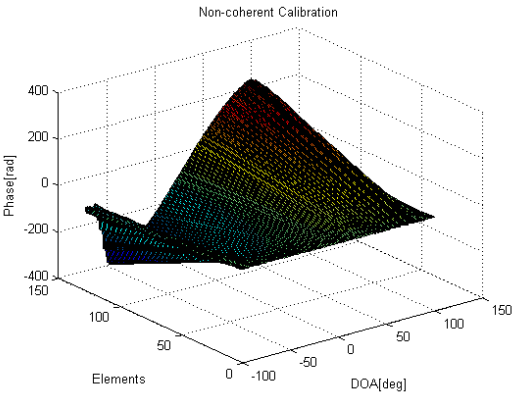

Fig. 8. Non-coherent calibration
Phase of the estimated array response
f_c=250KHz, DOA=[-100, 100] deg

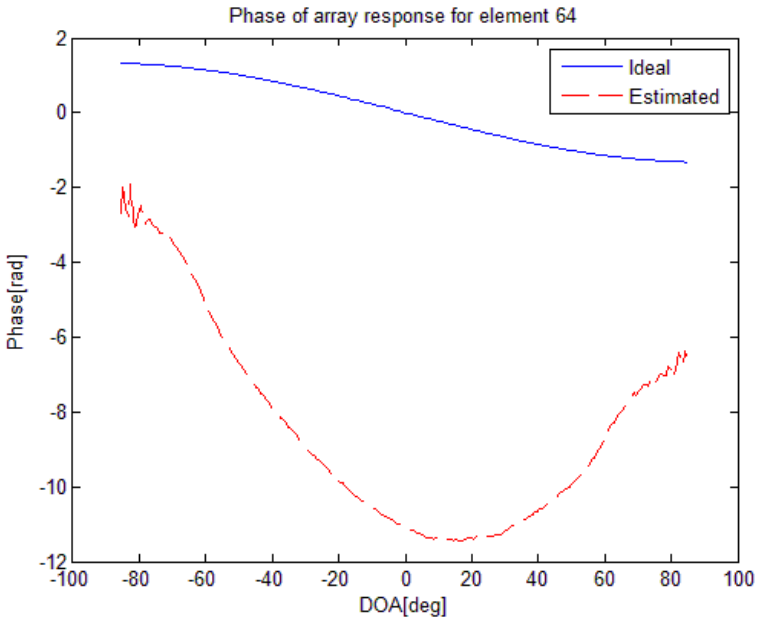

Fig. 9. Phase of the ideal and estimated array response for element 64

Figures 10, 11, 12 and 13 show the performance when using the ideal array response $\mathbf{A}$ and estimated array response $\widehat{\mathbf{A}}_{\mathbf{c}}$ in the two DOA estimation methods, classical beamforming and MUSIC. Figures 10 and 11 use the estimated array response from coherent calibration, Figures 12 and 13 use the estimated array response from non-coherent calibration. Figures 10, 12 and Figures 11, 13 are similar, which also proves that the $\widehat{\mathbf{A}}_{\mathbf{c}}$ obtained from the two methods are almost the same. So in the following analysis, only the estimated array response from the coherent calibration method is used. In these figures, the spectrum when using the ideal array response matrix $\mathbf{A}$ is very close to the one using the estimated ''real'' array response matrix $\widehat{\mathbf{A}}_{\mathbf{c}}$. Comparing the two DOA estimation methods, MUSIC has higher resolution than the beamforming method. And for the classical beamforming method, the two curves are close to each other, it is hard to distinguish which one has lower side lobe level.

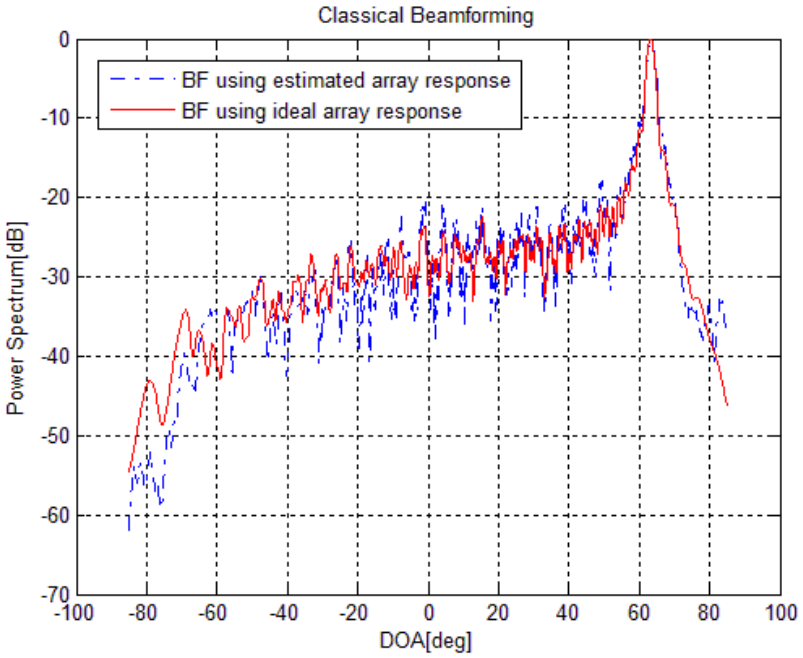

Fig. 10. Coherent calibration

Classical Beamforming method. Signal's angle of incidence is 63.49 degree.

Estimated direction using estimated array response is 63.60 degree.

Estimated direction using ideal array response is 63.20 degree.

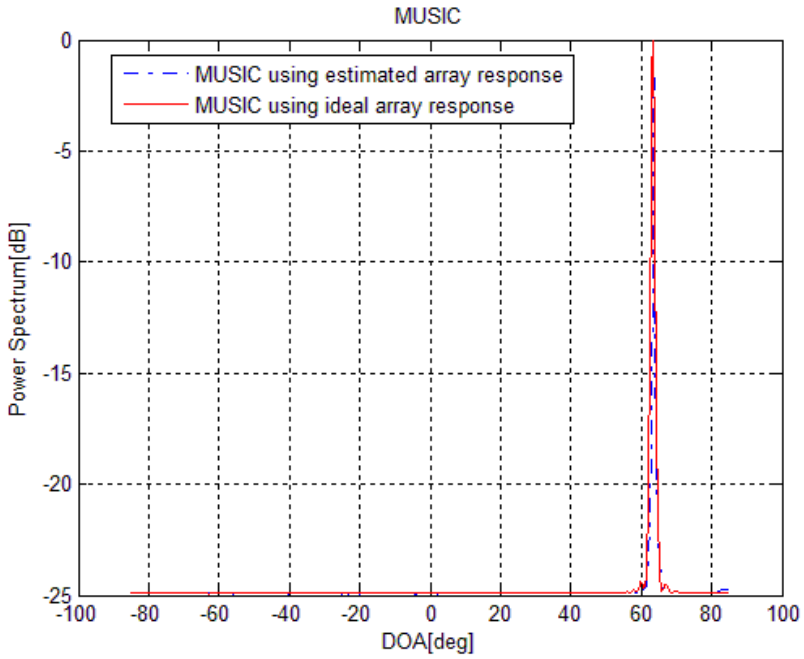

Fig. 11. Coherent calibration

MUSIC method. Signal's angle of incidence is 63.49 degree,

Estimated direction using estimated array response is 63.60 degree,

Estimated direction using ideal array response is 63.30 degree.

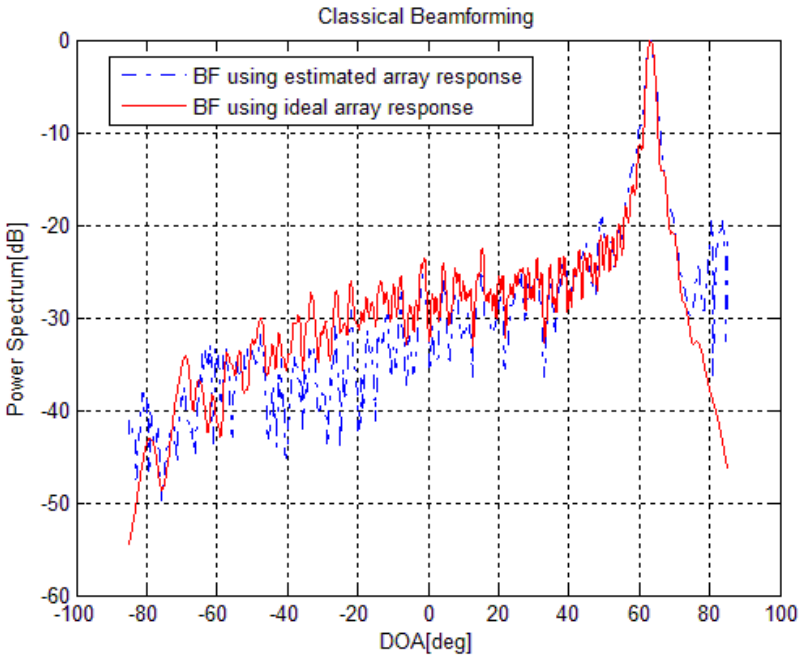

Fig. 12. Non_coherent calibration

Classical Beamforming method. Signal's angle of incidence is 63.49 degree,

Estimated direction using estimated array response is 62.80 degree,

Estimated direction using ideal array response is 63.20 degree.

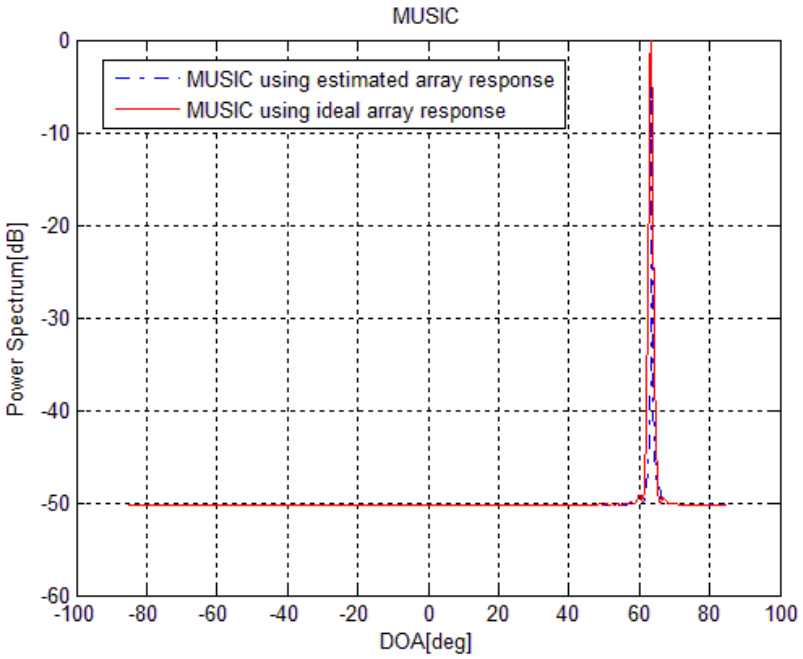

Fig. 13. Non_ coherent calibration

MUSIC method. Signal's angle of incidence is 63.49 degree,
Estimated direction using estimated array response is 63.50 degree,
Estimated direction using ideal array response is 63.30 degree.

5.3 Global calibration

The purpose of calibration is to correct errors which could not be considered when setting up the ideal array response model, such as element's position deviation, unknown mutual coupling and channel errors. The correction matrix **Q** is used to compensate these errors, expressed as $\widehat{\mathbf{A}}_c = \mathbf{QA}$. It is generally obtained by dividing the "real" array response by the ideal array response, but according to the different calibration models, there are different ways to perform this task.

In these two global calibration models introduced in Section 4.2, **Q** is a fixed matrix for all DOAs, it's simple and efficient when there are no DOA-dependent errors.

5.3.1 Global diagonal matrix calibration

The diagonal global calibration matrix can be computed as in (26). Here $\mathbf{A}(\theta_c)$ is the ideal array response shown in figures 3-4, and $\widehat{\mathbf{A}}_\mathbf{c}$ is the estimated array response shown in figures 5-6 (using coherent calibration results). Both of them are 128×C matrixes. $\widehat{\mathbf{A}}_{\mathbf{c,m}}$ and $\mathbf{A_m}(\boldsymbol{\theta}_\mathbf{c})$ denote the *m*-th row of corresponding matrix.

Figures 14 and 15 show the amplitude and phase of corrected array response, which is computed as $\widehat{\mathbf{Q}}_{\mathbf{diag}}\mathbf{A}$. The effects of the correction matrix can be seen by comparing to the ideal array response in Figures 3 and 4. Obviously the gain of the corrected array response is less smooth than the the ideal one.

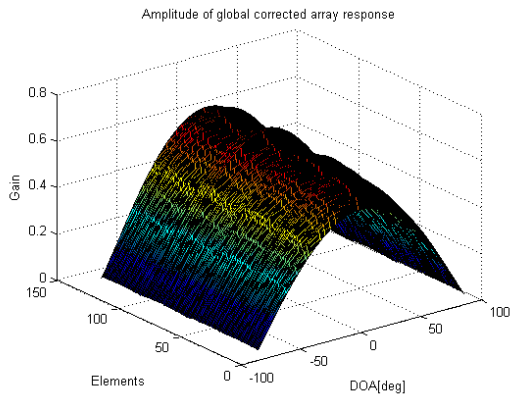

Fig. 14. Global diagonal matrix calibration Amplitude of the corrected array response

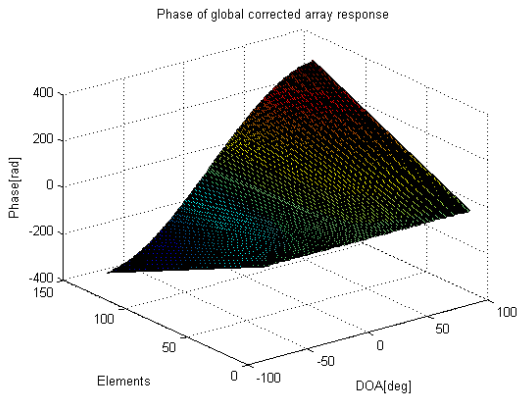

Fig. 15. Global diagonal matrix calibration Phase of the corrected array response

Figures 16 and 17 display the amplitude and phase of the ideal array response, estimated array response and corrected array response for element 64. These figures illustrate that the diagonal global calibration method cannot compensate for the model errors very well.

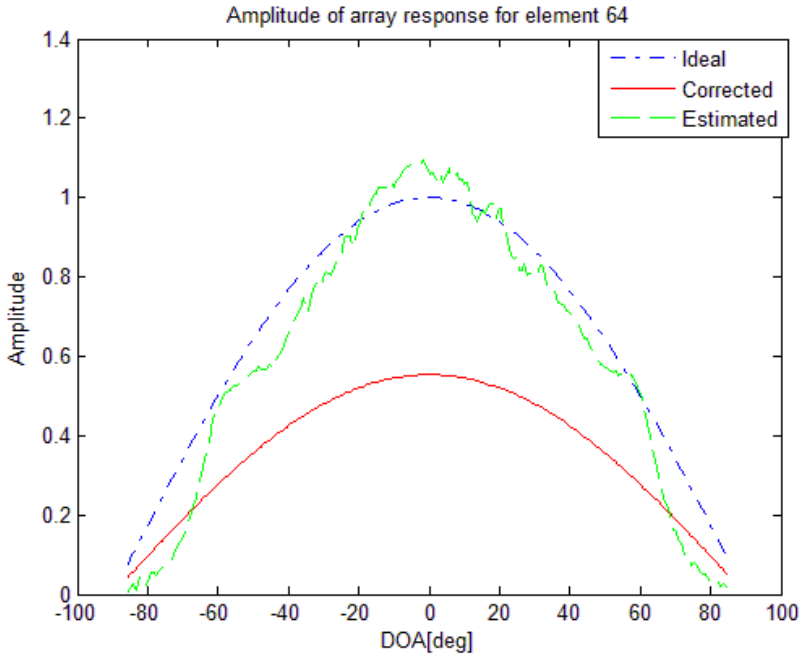

Fig. 16. Global diagonal matrix calibration
Comparison of the amplitude of array response for element 64

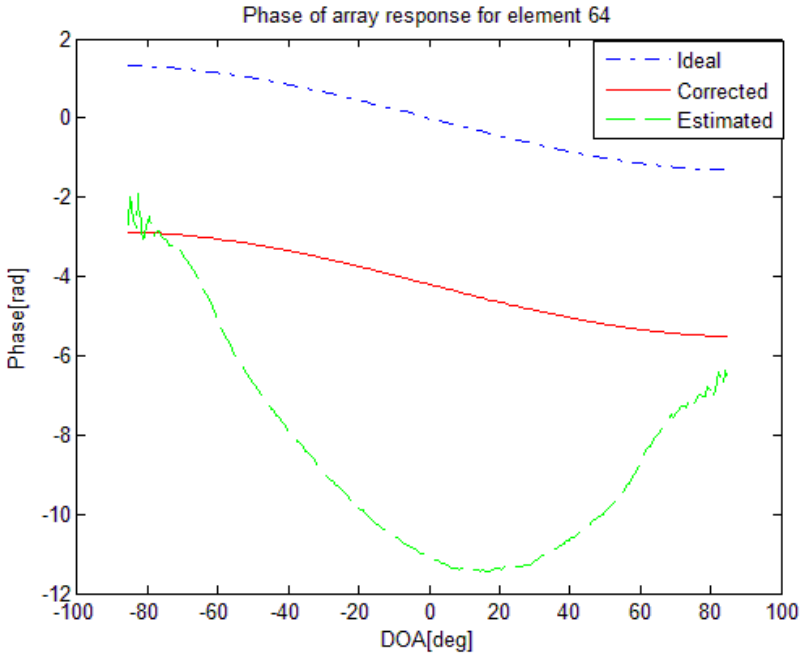

Fig. 17. Global diagonal matrix calibration
Comparison of the phase of array response for element 64

5.3.2 Global full matrix calibration

Global calibration using a full matrix works better than the diagonal one, since it can compensate not only for the channel errors but also for the unknown mutual coupling.

$$\widehat{\mathbf{Q}} = \widehat{\mathbf{A}}_{\mathbf{c}}\mathbf{A}^{*}(\boldsymbol{\theta}_{\mathbf{c}})(\mathbf{A}(\boldsymbol{\theta}_{\mathbf{c}})\mathbf{A}^{*}(\boldsymbol{\theta}_{\mathbf{c}}))^{-1} \tag{32}$$

$\widehat{\mathbf{Q}}$ can be computed as in (32). It can also be implemented as $\widehat{\mathbf{A}}_{\mathbf{c}} * \text{pinv}(\mathbf{A}(\boldsymbol{\theta}_{\mathbf{c}}))$ in MATLAB to avoid numerical problems. Figures 18 and 19 illustrate the estimated correction matrix $\widehat{\mathbf{Q}}$.

In Figure 18, the maximum amplitude of the correction matrix $\widehat{\mathbf{Q}}$ is around 1.5×10^{11}, which is extremely huge and means that the results are meaningless.

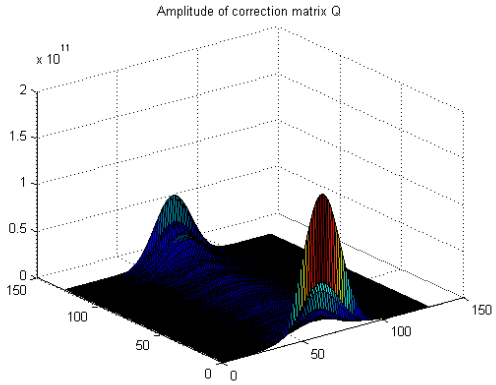

Fig.18. Global full matrix calibration Amplitude of the correction matrix

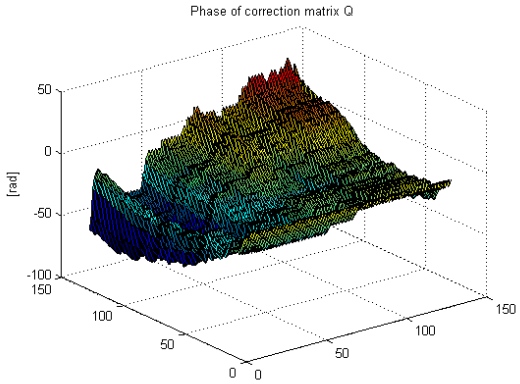

Fig. 19. Global full matrix calibration Phase of the correction matrix

After some analysis, we found that this may be because the simulated ideal array response $\mathbf{A}(\boldsymbol{\theta}_{\mathbf{c}})$ is not full rank. Computing the singular value decomposition (SVD) as follows,

$$\mathbf{A}(\boldsymbol{\theta}_{\mathbf{c}})=\mathbf{U}\boldsymbol{\Sigma}\mathbf{V}^{*}, \tag{33}$$

where $\mathbf{U}$ is a M×M complex unitary matrix, and $\boldsymbol{\Sigma}$ is a M×C rectangular diagonal matrix with nonnegative real numbers on the diagonal, it can be expressed as $\boldsymbol{\Sigma} = \left[\begin{array}{cccc|cc} \delta_1 & 0 & 0 & 0 & 0 & 0 \\ 0 & \delta_2 & 0 & 0 & 0 & 0 \\ 0 & 0 & \ddots & 0 & 0 & 0 \\ 0 & 0 & 0 & \delta_m & 0 & 0 \end{array}\right]$, $\mathbf{V}^{*}$ (the conjugate transpose of $\mathbf{V}$) is a C×C complex unitary matrix. The rank of $\mathbf{A}(\boldsymbol{\theta}_{\mathbf{c}})$ equals the number of

non-zero singular values, which is the same as the number of non-zero diagonal elements in $\mathbf{\Sigma}$.

Figure 20 plots the singular values $\mathbf{S}=[\delta_1, \delta_2, \ldots, \delta_m]$. The minimum singular value is close to 10^{-12}. When computing the correction matrix $\widehat{\mathbf{Q}}$ by $\widehat{\mathbf{A}}_\mathbf{c}/\mathbf{A}(\boldsymbol{\theta}_\mathbf{c})$, or $\widehat{\mathbf{A}}_\mathbf{c}$ pinv$(\mathbf{A}(\boldsymbol{\theta}_\mathbf{c}))$, it makes the amplitude of $\widehat{\mathbf{Q}}$ to be as huge as 10^{12}.

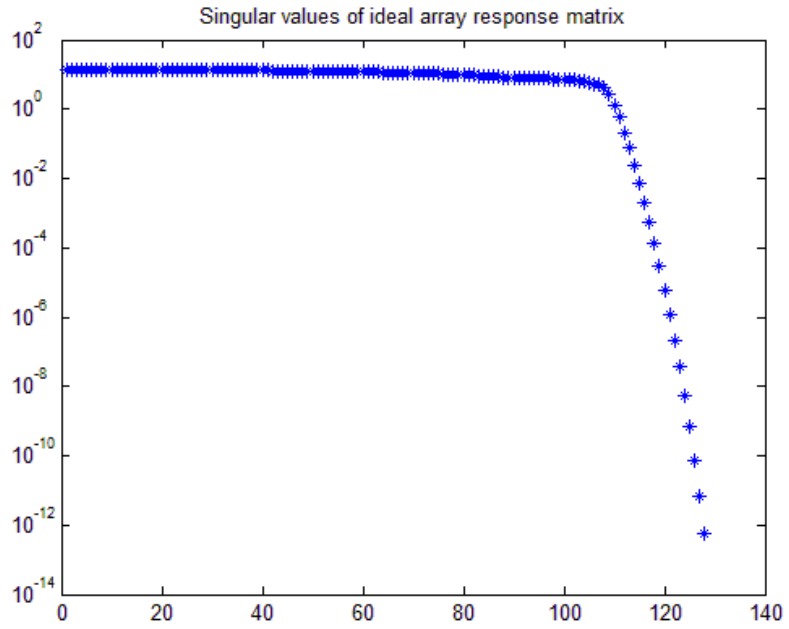

Fig. 20. Singular values of ideal array response matrix

There are two ways to solve this problem:

a) one solution is to set a tolerance value in $\widehat{\mathbf{A}}_\mathbf{c} *$ pinv $(\mathbf{A}(\boldsymbol{\theta}_\mathbf{c})$, tol). Thus, all the singular values less than 'tol' will be treated as zero.

b) the other solution is to use so-called regularization [8].

$$\widehat{\mathbf{Q}} = \widehat{\mathbf{A}}_\mathbf{c}\mathbf{A}^*(\boldsymbol{\theta}_\mathbf{c})(\mathbf{A}(\boldsymbol{\theta}_\mathbf{c})\mathbf{A}^*(\boldsymbol{\theta}_\mathbf{c}) + \lambda\mathbf{I})^{-1}, \tag{34}$$

where λ is called the regularization parameter that can be set as 1, 0.1 or other suitable values. Further, $\mathbf{I}$ is a M×M identity matrix. In this way, a small value is added on the singular values shown in Figure 20, which influences little on the large singular values but move the small singular values away from zero. Figures 21 and 22 show the correction matrix $\widehat{\mathbf{Q}}$ computed by (34) using $\lambda = 0.1$. This $\widehat{\mathbf{Q}}$ is a diagonal dominated matrix as we expected. Because the full correction matrix can compensate for the mutual coupling, and theoretically, the mutual coupling between

neighboring elements is much stronger than the one between distant elements, so as a compensation for the ideal array response, the reasonable $\hat{\mathbf{Q}}$ should be a diagonal dominated matrix.

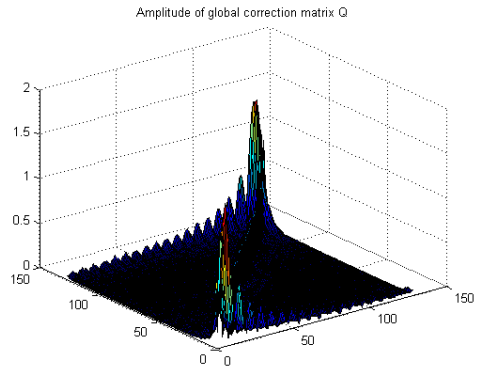

Fig.21. Global full matrix calibration
Amplitude of the correction matrix

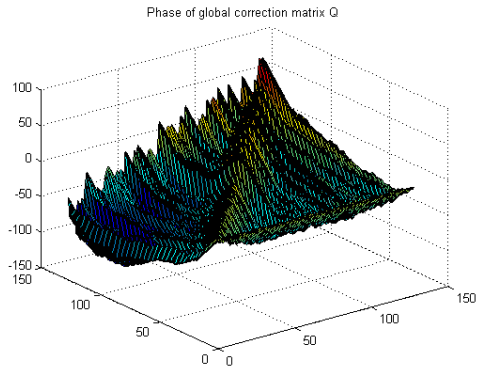

Fig.22. Global full matrix calibration
Phase of the correction matrix

By using this estimated $\hat{\mathbf{Q}}$ to correct the model errors, we get a corrected array response which is close to the 'real' array response as shown in figures 23 and 24.

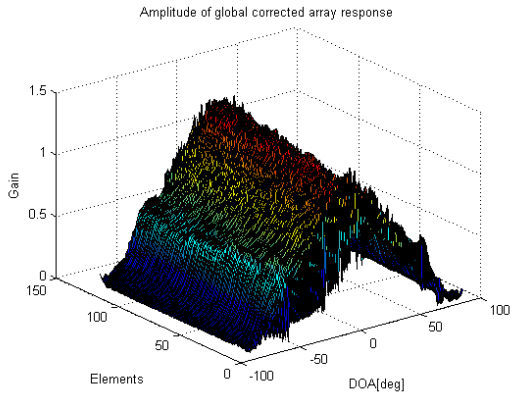

Fig. 23. Global full matrix calibration
Amplitude of the corrected array response

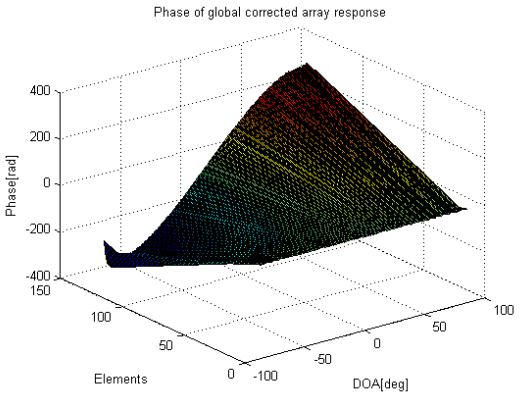

Fig. 24. Global full matrix calibration
Phase of the corrected array response

Figures 25 and 26 also plot the array response for element 64 as a comparison. The corrected array response is very close to the estimated one in both amplitude and phase.

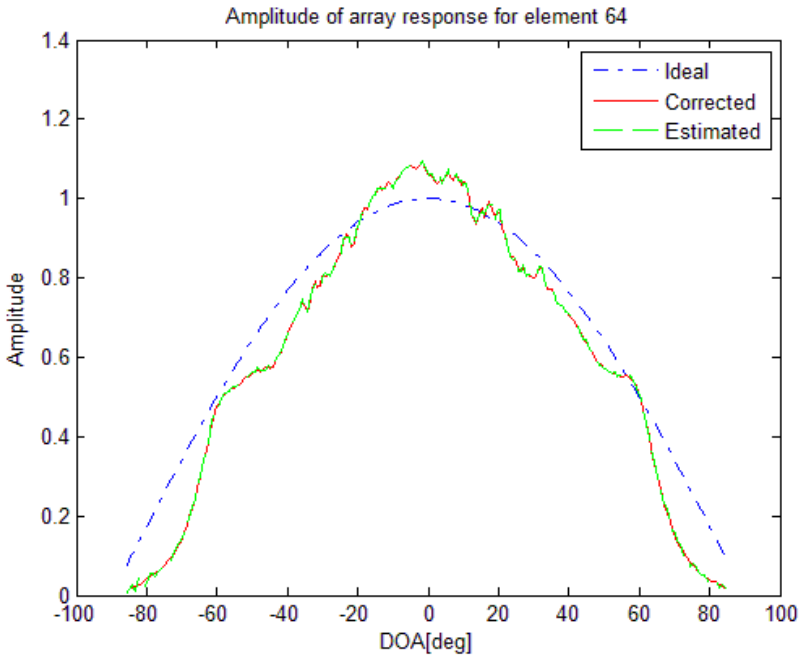

Fig. 25. Global full matrix calibration
Comparison of the amplitude of array response for element 64

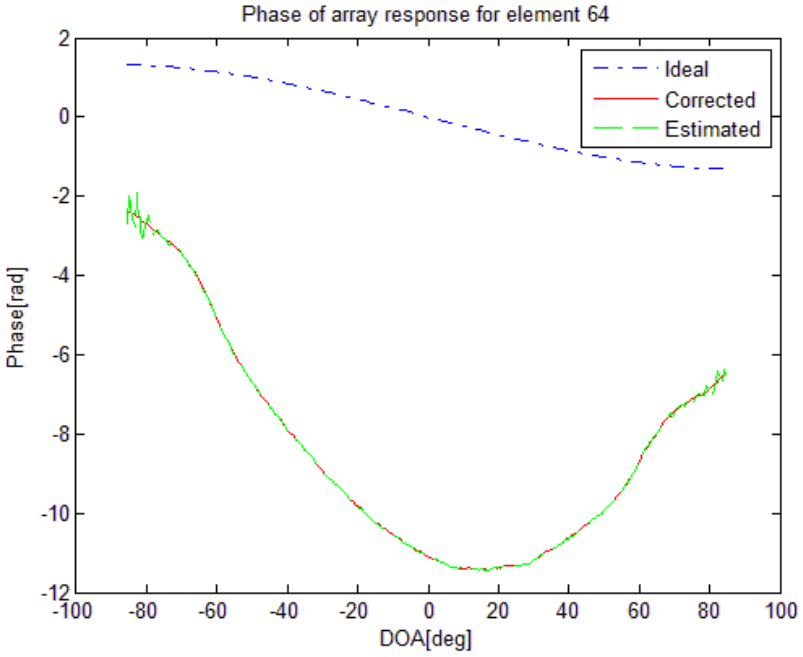

Fig. 26. Global full matrix calibration
Comparison of the phase of array response for element 64

5.4 Local calibration

Compared with global calibration methods, local calibration is more complicated. The local calibration method exploits a DOA-dependent matrix $\hat{\mathbf{q}}(\theta_c)$, which is computed as in (29). The real part and imaginary part of $\hat{\mathbf{q}}(\theta_c)$ are shown in Figures 27 and 28. It satisfies the only requirement for local calibration, that is $\hat{\mathbf{q}}(\theta_c)$ should be a smooth function of the DOA θ_c to be useful.

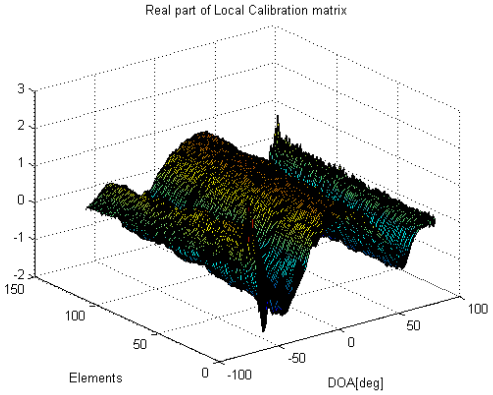

Fig.27. Local calibration
The real part of $\hat{q}(\theta_c)$

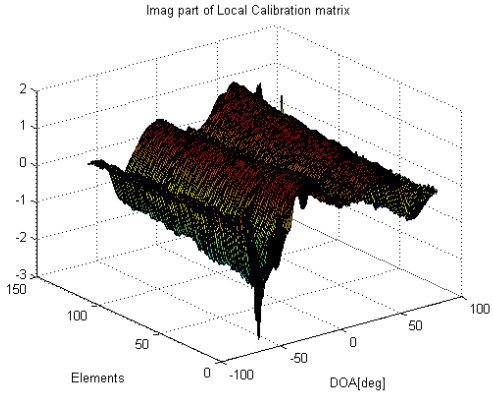

Fig.28. Local calibration
The imaginary part of $\hat{q}(\theta_c)$

Then, linear interpolation can be performed on $\hat{\mathbf{q}}(\theta_c)$ to obtain the correction matrix for any desired θ. The interesting DOA range in this case is [-80 80], with intervals of 0.1 degree. Figures 29 and 30 show the corrected array response using a local calibration matrix. It is very close to the estimated array response, which means that the local calibration method compensated the model errors very well.

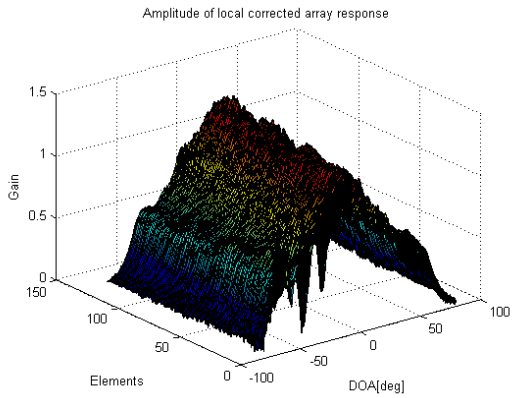

Fig. 29. Local calibration
Amplitude of the corrected array response

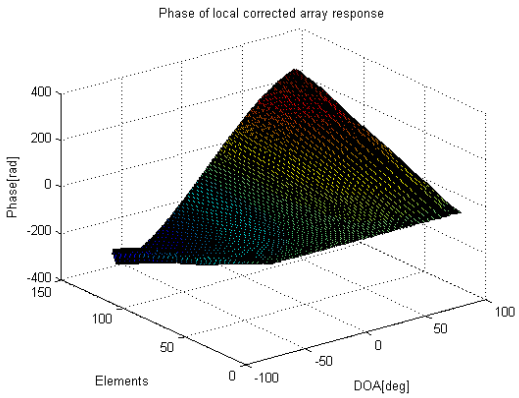

Fig. 30. Local calibration
Phase of the corrected array response

For the local calibration method, the three array responses are also shown in Figures 31 and 32. The corrected array response coincides with the estimated array response.

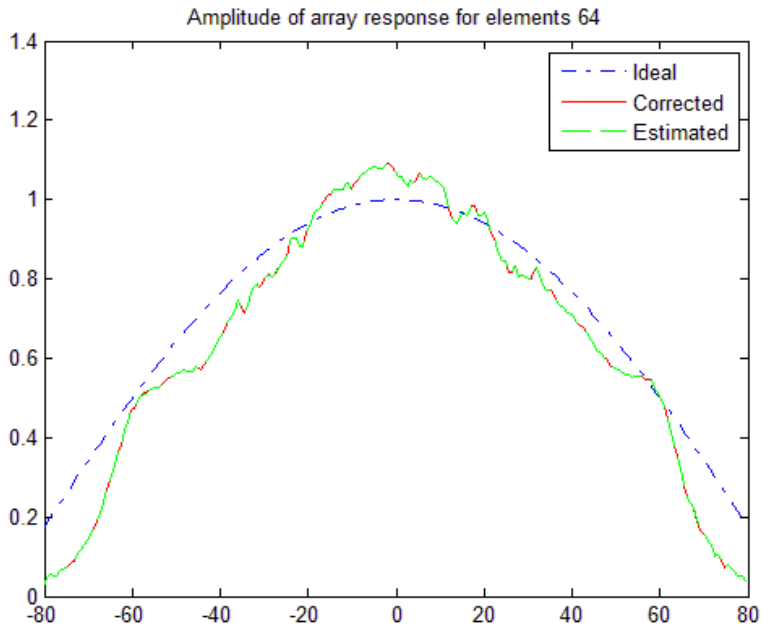

Fig. 31. Local calibration
Comparison of the amplitude of array response for element 64

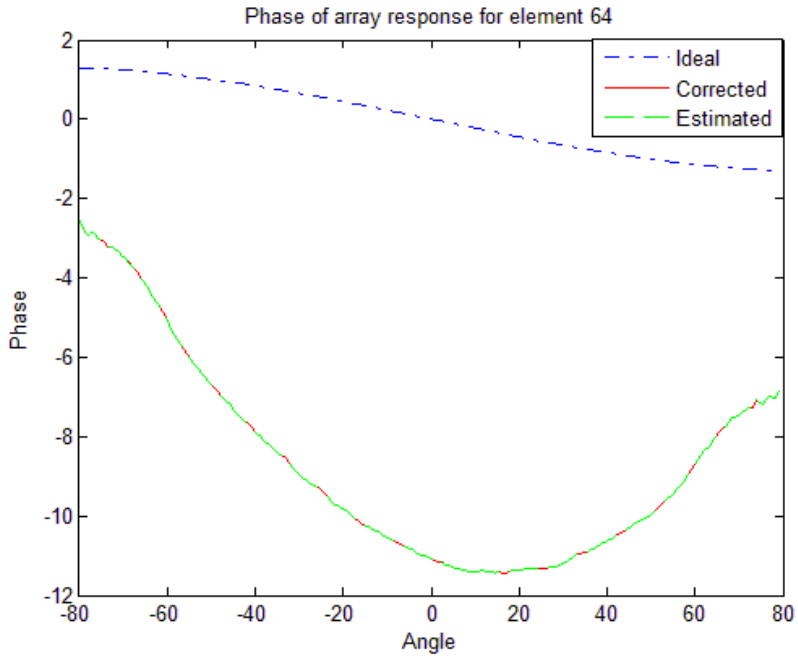

Fig. 32. Local calibration
Comparison of the phase of array response for element 64

5.5 Performance comparison.

In order to compare the accuracy of DOA estimation, the average DOA RMS error Δ is defined as

$$\Delta=\sqrt{\frac{\sum_{c=1}^{C}(\hat{\theta}_c-\theta_c)^2}{C}}, \tag{35}$$

where $\hat{\theta}_c$ is the estimated direction at position c, and θ_c denotes the real direction. But gross errors exist in the estimated DOAs as shown in Figure 33. The signal comes from 60 degree direction in one experiment, but the estimated DOA is -60 degree. This error is regarded as gross error. In order to obtain a robust approach to describe the performances of calibration methods, we remove the five maximum and minimum errors, and then compute the DOA RMS error Δ as (35).

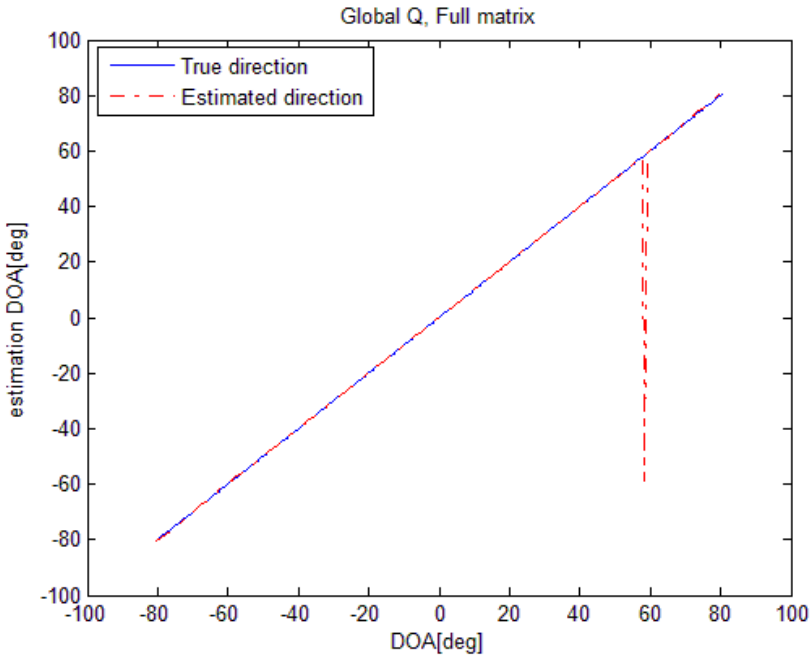

Fig. 33. Estimated directions using global full matrix calibration
$\hat{\mathbf{Q}}$ is obtained from dataset 112, $\mathbf{x}[n]$ is obtained from dataset 124
f_c = 350 KHz

Table 1 states the results when using the three different calibration ways: global diagonal matrix calibration, global full matrix calibration and local calibration. $\hat{\mathbf{Q}}$ is computed by using dataset 112. Comparing with the cases without calibration, the diagonal matrix method results in larger DOA RMS errors, it fails to improve the performance of DOA estimation. The full matrix calibration only works on dataset 124 when the DOA range is [-80 80] deg.

The local calibration method achieves good performance for the entire datasets. It returns the corrected steering vectors $\widehat{\mathbf{Q}}(\boldsymbol{\theta})\mathbf{a}(\boldsymbol{\theta})$, which are almost collinear to the estimated ''real'' steering vectors $\hat{\mathbf{a}}(\boldsymbol{\theta})$.

Table 1 DOA RMS error Δ
($\widehat{\mathbf{Q}}$ is obtained from dataset 112, f_c=250KHz, $\theta_c = [-80\ 80]$deg)

Datasets	112	124	125
Diagonal matrix calibration	0.1122 deg	0.1752 deg	0.1588 deg
Full matrix calibration	0.2347 deg	0.1082 deg	0.2015 deg
Local calibration	0.0288 deg	0.0759 deg	0.0834 deg
Without calibration	0.0964 deg	0.1664 deg	0.1427 deg

If we decrease the range by setting $\theta_c = [-70\ 70]$ deg, as shown in Table 2, the global full matrix calibration method does improve the estimation accuracy on the three datasets. From this we also conclude that it is more difficult to correct errors near the limits of the useful DOA range.

Table 2 DOA RMS error Δ
($\widehat{\mathbf{Q}}$ is obtained from dataset 112, f_c=250KHz, $\theta_c = [-70\ 70]$deg)

Datasets	112	124	125
Diagonal matrix calibration	0.0964 deg	0.1377 deg	0.1284 deg
Full matrix calibration	0.0439 deg	0.0498 deg	0.0478 deg
Local calibration	0.0285 deg	0.0568 deg	0.0524 deg
Without calibration	0.0934 deg	0.1352 deg	0.1178 deg

Datasets 124_1, 124_2 and 124_3 are three independent measurements using the very same arrays. Table 3 shows the results when applying the calibration matrix obtained from 124_1 on the other two independent measurements. For DOA range [-80 80] deg, the global full matrix calibration still doesn't work, while local calibration perform very well.

Table 3 DOA RMS error Δ
($\widehat{\mathbf{Q}}$ is obtained from dataset 124_1, f_c=250 KHz, $\theta_c = [-80\ 80]$deg)

Datasets	124_1	124_2	124_3
Global full matrix calibration	0.1633 deg	0.1679 deg	0.1453 deg
Local calibration	0.0290 deg	0.0322 deg	0.0337 deg
Without calibration	0.0764 deg	0.0798 deg	0.0782 deg

Table 4 shows the results after decreasing the DOA range as [-70 70] deg, global full matrix calibration improves the performance significantly.

Table 4 DOA RMS error Δ
($\widehat{\mathbf{Q}}$ is obtained from dataset 124_1, f_c=250 KHz, $\theta_c = [-70\ 70]$deg)

Datasets	124_1	124_2	124_3
Global full matrix calibration	0.0433 deg	0.0454 deg	0.0411 deg
Local calibration	0.0495 deg	0.0380 deg	0.0359 deg
Without calibration	0.0717 deg	0.0784 deg	0.0770 deg

To compare the improvements more straightly, we calculate the percentage of improvements as $(\Delta\text{-}\Delta_c)/\Delta$. Here, Δ is the DOA RMS error without calibration, and Δ_c is the DOA RMS error with calibration.

As a conclusion, for DOA range [-80 80] degree, the local calibration method can improve the estimation accuracy 34%, global calibration methods don't work in this case. For DOA range [-70 70] degree, global full matrix method achieved similar performance (50% improvement) as local calibration method (53% improvement). Obviously, the local calibration method is comparatively robust to different modeling errors and improves the performance superiorly.

5.6 Frequency dependency of the array response

Figures 34-41 indicate that the array response of this array is frequency dependent. By increasing the carrier frequency f_c from 200 KHz to 400 KHz, the estimated array response is varying.

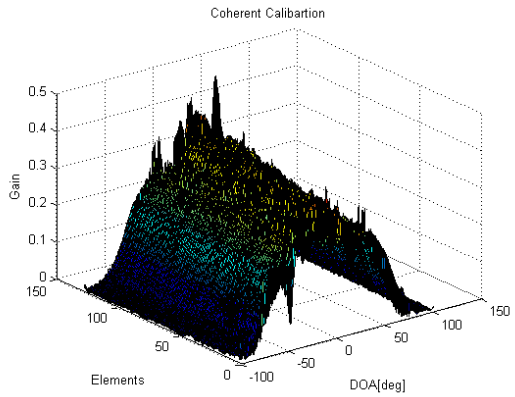

Fig. 34. Gain of the estimated array response f_c= 200 KHz, DOA=[-100, 100] deg

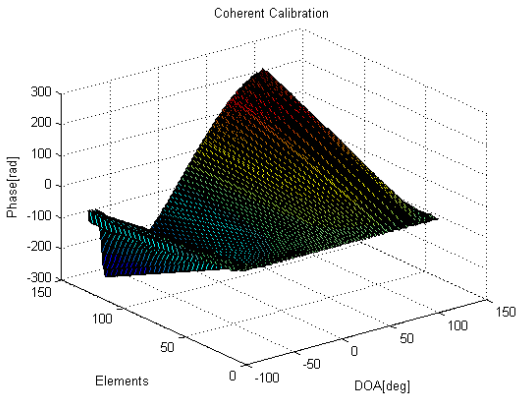

Fig. 35. Phase of the estimated array response f_c= 200 KHz, DOA=[-100, 100] deg

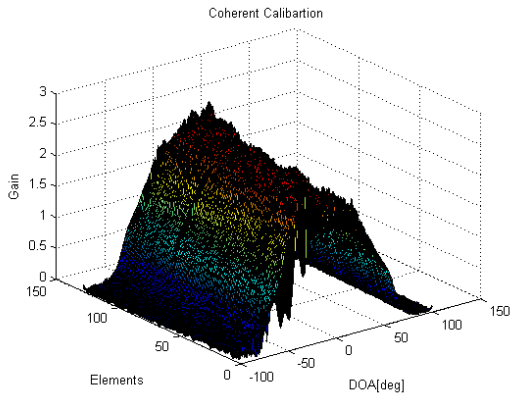

Fig. 36. Gain of the estimated array response f_c= 300 KHz, DOA=[-100, 100] deg

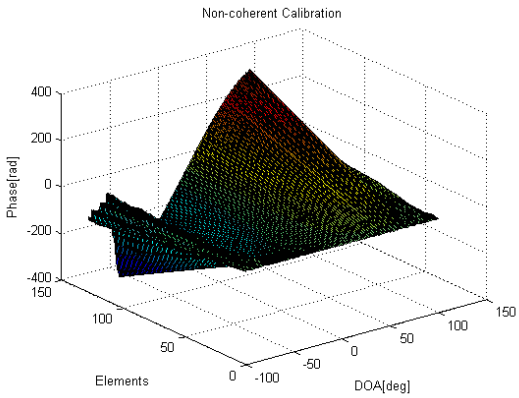

Fig. 37. Phase of the estimated array response f_c= 300 KHz, DOA=[-100, 100] deg

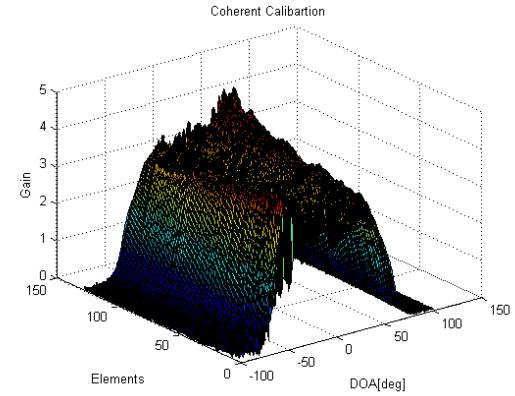

Fig. 38. Gain of the estimated array response f_c= 350 KHz, DOA=[-100, 100] deg

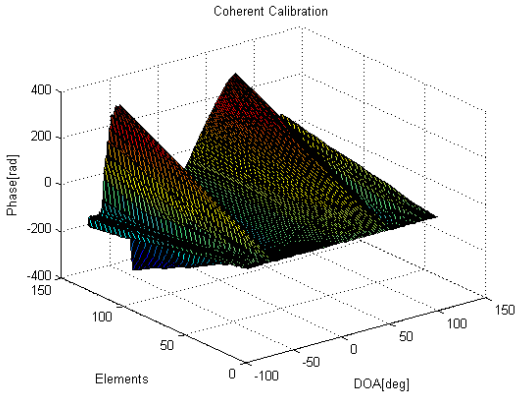

Fig. 39. Phase of the estimated array response f_c= 350 KHz, DOA=[-100, 100] deg

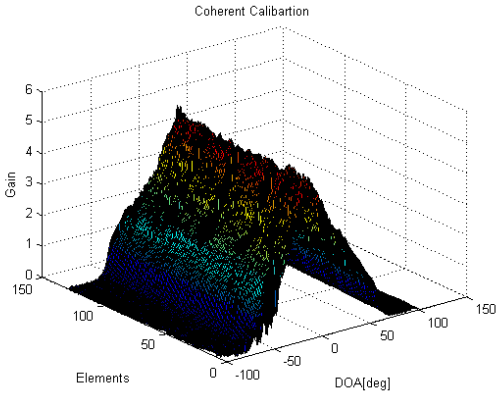

Fig. 40. Gain of the estimated array response f_c= 400 KHz, DOA=[-100, 100] deg

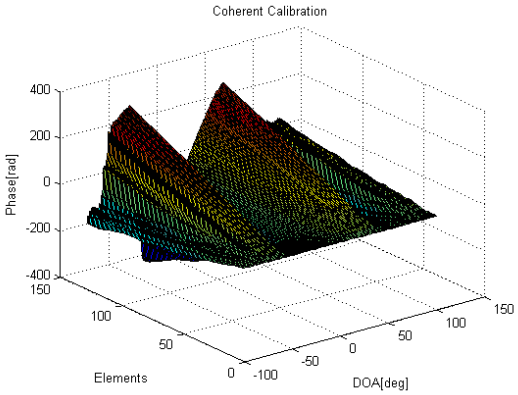

Fig. 41. Phase of the estimated array response f_c= 400 KHz, DOA=[-100, 100] deg

Using the global full matrix calibration method on dataset 112 with different f_c (200 KHz, 250 KHz, 300 KHz, 350 KHz, and 400 KHz); Figures 42-51 show the corresponding correction matrix $\hat{\mathbf{Q}}$. Obviously, $\hat{\mathbf{Q}}$ is also varying with f_c, which means that the mutual coupling between elements is affected by carrier frequency.

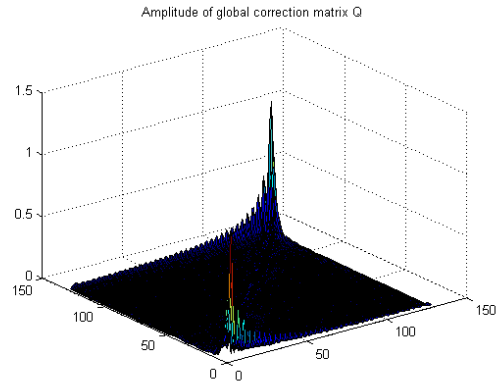

Fig. 42. Amplitude of the correction matrix f_c= 200 KHz

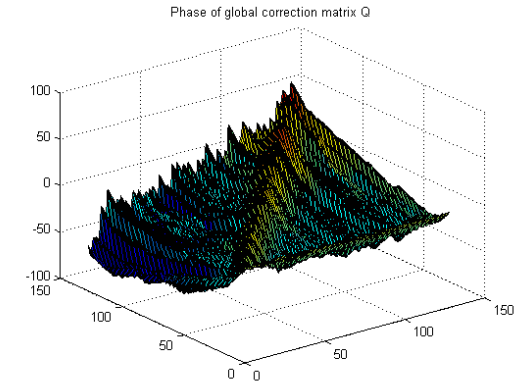

Fig. 43. Phase of the correction matrix f_c= 200 KHz

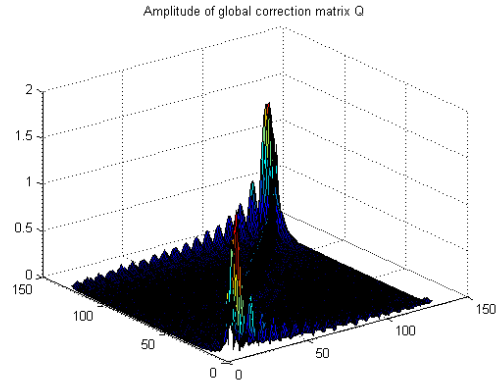

Fig. 44. Amplitude of the correction matrix f_c= 250 KHz

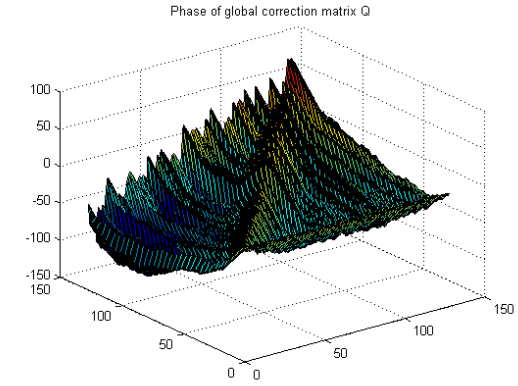

Fig. 45. Phase of the correction matrix f_c= 250 KHz

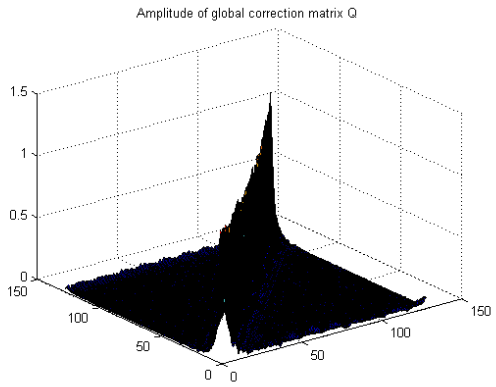

Fig. 46. Amplitude of the correction matrix f_c= 300 KHz

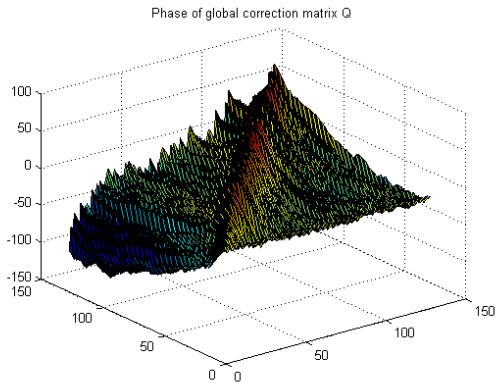

Fig. 47. Phase of the correction matrix f_c= 300 KHz

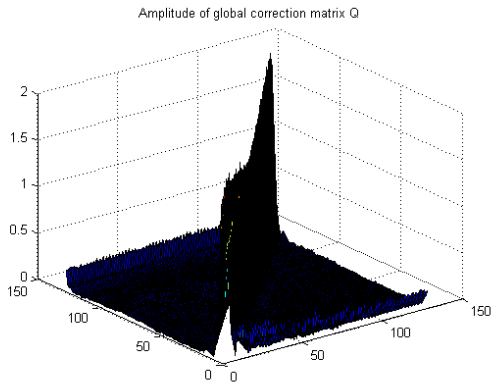

Fig. 48. Amplitude of the correction matrix f_c= 350 KHz

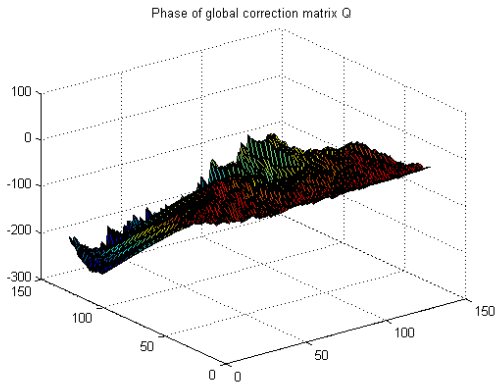

Fig. 49. Phase of the correction matrix f_c= 350 KHz

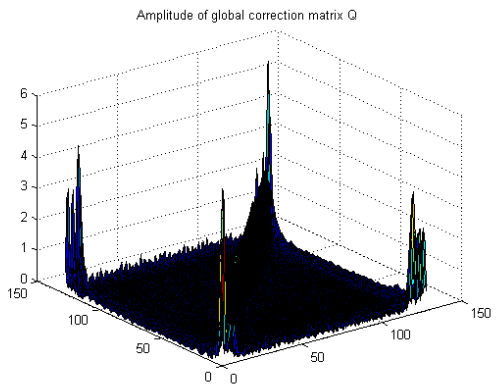

Fig. 50. Amplitude of the correction matrix f_c= 400 KHz

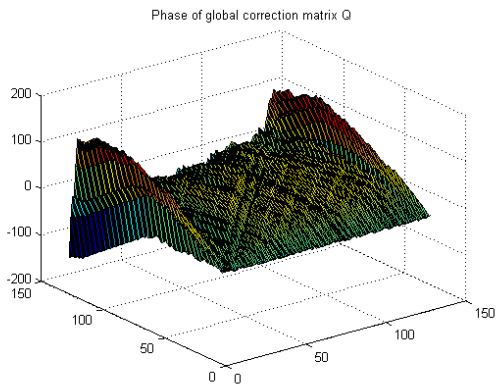

Fig. 51. Phase of the correction matrix f_c= 400 KHz

Figures 52-59 plot the corrected array response by using the calibration matrix $\widehat{\mathbf{Q}}$ in the ideal model. The correction matrix $\widehat{\mathbf{Q}}$ works for f_c= 200 KHz. As shown in Figures 52 and 53, the corrected array response perfectly coincides with the estimated array response. The case of f_c=250 KHz has been discussed in section 5.3.2, it also works very well.

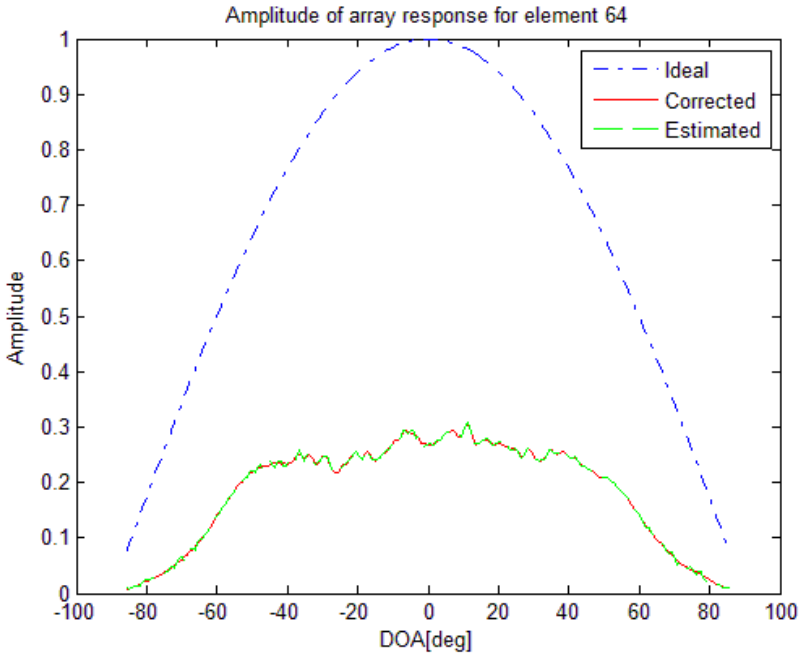

Fig. 52. Amplitude of array response for element 64
Global full matrix calibration, f_c = 200 KHz

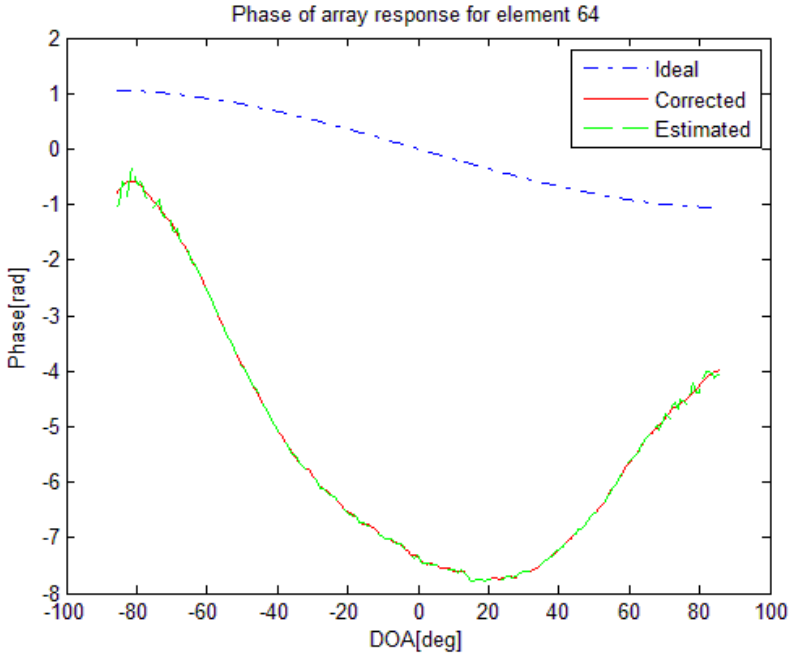

Fig. 53. Phase of array response for element 64
Global full matrix calibration, f_c = 200 KHz

Figures 54 and 55 show that this global calibration method can only compensate for the amplitude error for f_c= 300 KHz, it is not perfect for the phase error compensation.

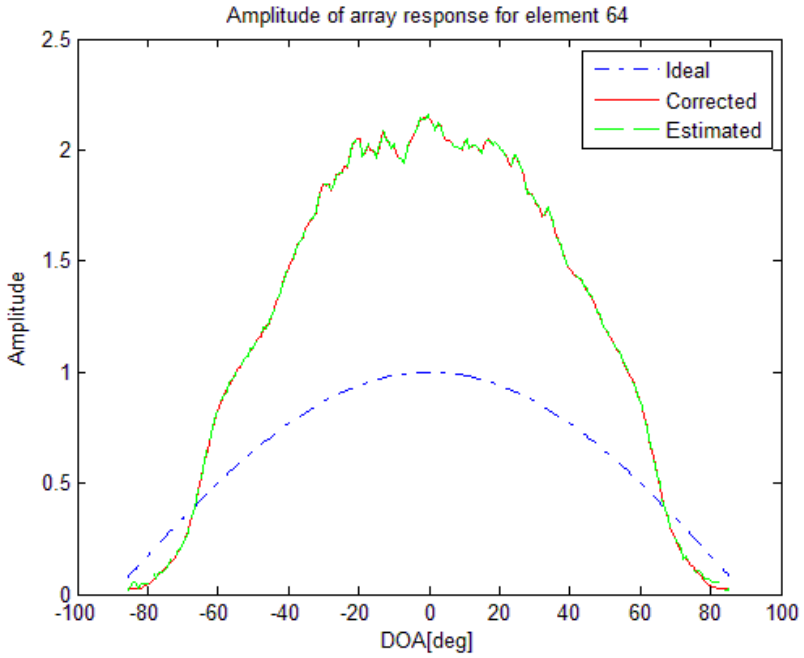

Fig. 54. Amplitude of array response for element 64
Global full matrix calibration, f_c = 300 KHz

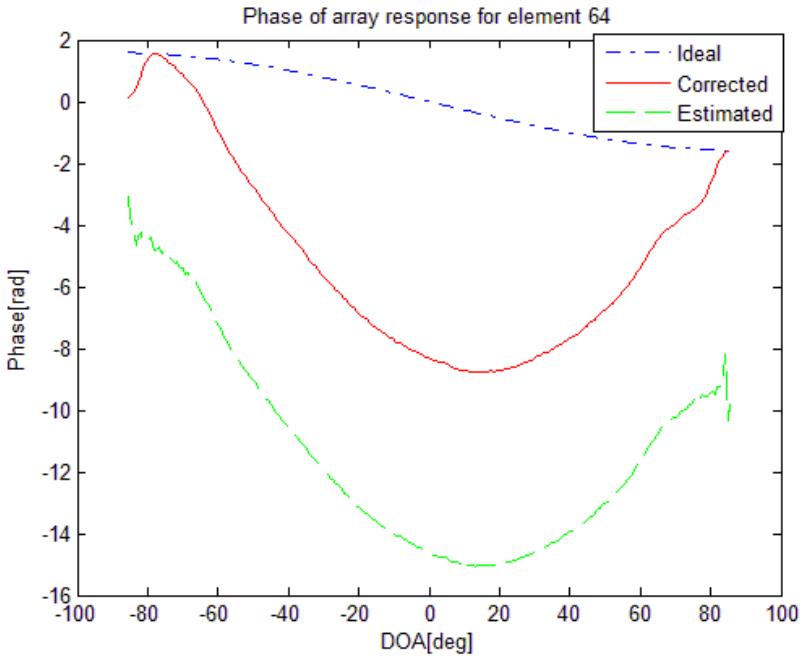

Fig. 55. Phase of array response for element 64
Global full matrix calibration, f_c= 300 KHz

In the cases of f_c = 350 KHz and f_c = 400 KHz, the corrected array response still deviates from the estimated "real" array response, especially in the edge of the DOA range, as shown in Figures 56-59. That means that this global calibration matrix $\widehat{\mathbf{Q}}$ cannot work very well to compensate the non-ideal properties when f_c is high.

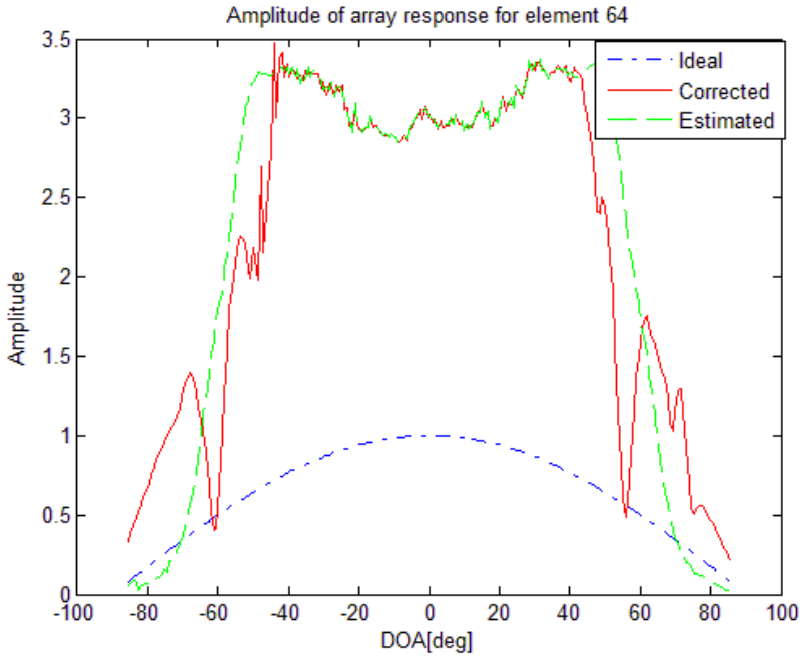

Fig. 56. Amplitude of array response for element 64
Global full matrix calibration, f_c = 350 KHz

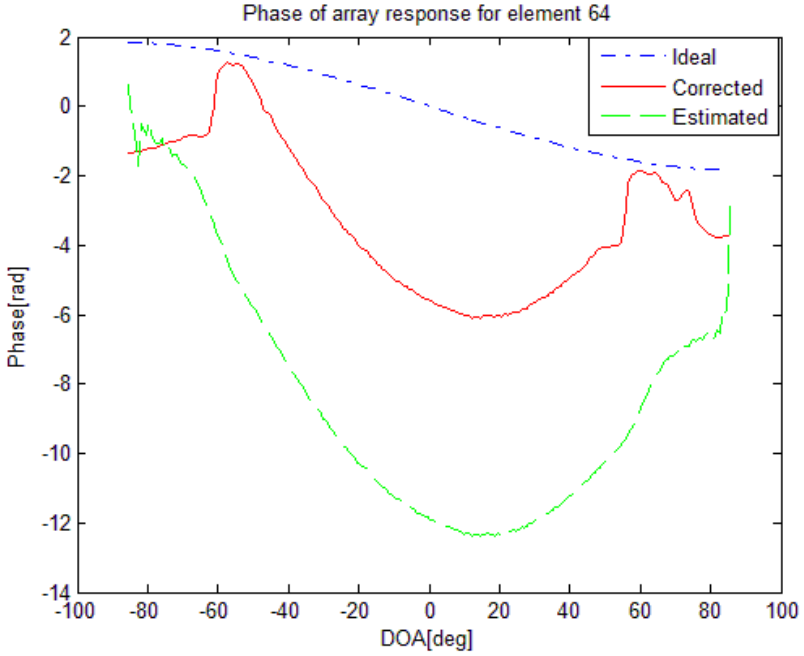

Fig. 57. Phase of array response for element 64
Global full matrix calibration, f_c = 350 KHz

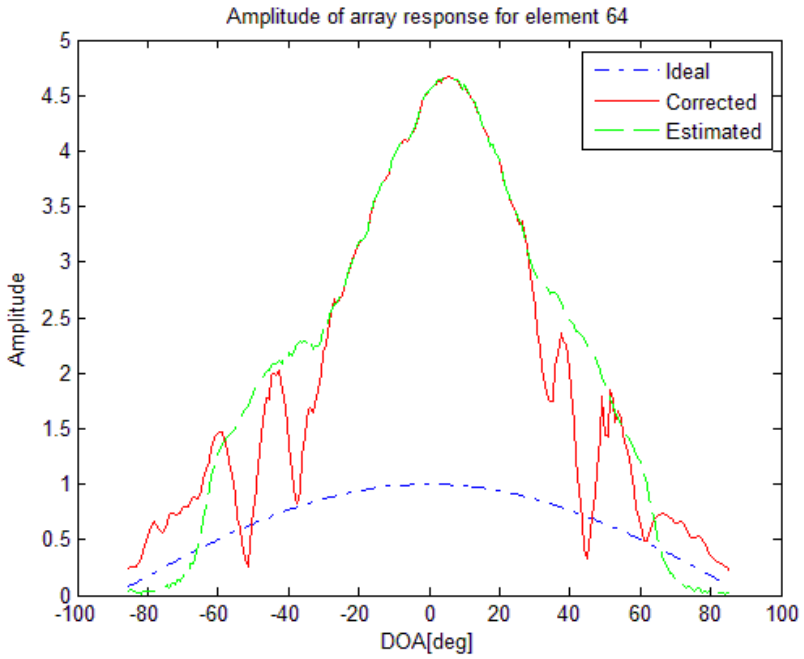

Fig. 58. Amplitude of array response for element 64
Global full matrix calibration, f_c = 400 KHz

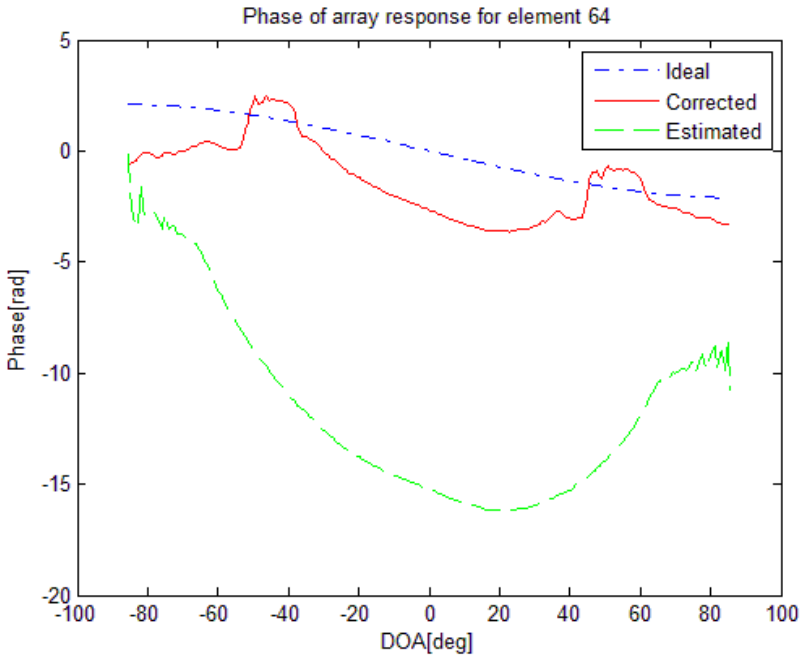

Fig. 59. Phase of array response for element 64
Global full matrix calibration, f_c= 400 KHz

Comparing to the global calibration method, local calibration is always effective for different carrier frequencies. Table 5 shows the performances of global full matrix calibration and local calibration when f_c is fixed to 200 KHz, 300 KHz, 350 KHz and 400 KHz. The full matrix calibration method doesn't work for any frequency when $\theta_c = [-80\ 80]\text{deg}$, but the local calibration method improves the estimation accuracy a lot.

Table 5 Global and Local Calibration, DOA RMS error
($\widehat{\mathbf{Q}}$ is obtained from dataset 112, $\mathbf{x}[n]$ is obtained from dataset 124, $\theta_c = [-80\ 80]\text{deg}$)

Frequency	200 KHz	300 KHz	350 KHz	400KHz
Full matrix calibration	0.0817 deg	0.1293 deg	0.1844 deg	0.1740 deg
Local calibration	0.0852 deg	0.0772 deg	0.0692 deg	0.0983 deg
Without calibration	0.1820 deg	0.1456 deg	0.1436 deg	0.1561 deg

In Table 6, the DOA range is changed to [-70 70] deg. The global full matrix calibration method works for every frequency in this DOA range. For some frequencies, it even has better performance.

Table 6 Global and Local Calibration, DOA RMS error
($\widehat{\mathbf{Q}}$ is obtained from dataset 112, $\mathbf{x}[n]$ is obtained from dataset 124, $\theta_c = [-70\ 70]\text{deg}$)

Frequency	200 KHz	300 KHz	350 KHz	400KHz
Full matrix calibration	0.0468 deg	0.0446 deg	0.1110 deg	0.0498 deg
Local calibration	0.0506 deg	0.0519 deg	0.0449 deg	0.0568 deg
Without calibration	0.1333 deg	0.1194 deg	0.1202 deg	0.1352 deg

Chapter 6 Further Discussion

Sections 4.1 and 4.2 describe two ways to estimate the ''real'' array response, they are coherent calibration and non-coherent calibration. Since the phase and gain of s(t) used in the coherent calibration method are unknown, we assume the gain is 1 and phase φ is 0° when generating s(t) in MATLAB. Due to this, the $\mathbf{x}_c(n)$ and $s_c(n)$ used in equation (21) are coherent, but with different amplitude and phase. Generally, coherent calibration will get a better performance than non-coherent calibration. But in this case, we get the same estimated array response from these two methods. In order to improve the performance of calibration, a new global calibration method with unknown phase and gain is proposed in [7]. This section will give a brief introduction of this newly-developed method, and also show some experimental results.

In local or global calibration, the correction matrix is achieved by using the least-square technique as follows:

$$\widehat{\mathbf{Q}} = \arg\min_{\mathbf{Q}} \left\| \widehat{\mathbf{A}}_{\mathbf{c}} - \mathbf{Q}\mathbf{A}(\theta_c) \right\|_F^2 , \tag{36}$$

where $\widehat{\mathbf{A}}_{\mathbf{c}} = [\hat{\mathbf{a}}(\theta_1)\ \hat{\mathbf{a}}(\theta_2) \dots \dots \hat{\mathbf{a}}(\theta_C)]$ and $\mathbf{A}(\theta_c) = [\mathbf{a}(\theta_1)\ \mathbf{a}(\theta_2) \dots \dots\ \mathbf{a}(\theta_c)]$ denote the estimated array response and ideal array response respectively. The subscript *F* means Frobenius norm.

Assume the estimated array response vector $\hat{\mathbf{a}}(\theta_c)$ have corresponding gain g_c and phase φ_c, then the unknown gain and phase can be represented as $r_c = g_c \exp(j\varphi_c)$. Let $\mathbf{\Gamma}$ be a diagonal matrix generated by the vector $[r_1\ r_2 \dots \dots \dots\ r_C]$,

$$\mathbf{\Gamma} = \begin{bmatrix} r_1 & 0 & 0 & 0 \\ 0 & r_2 & 0 & 0 \\ 0 & 0 & \dots\dots & 0 \\ 0 & 0 & 0 & r_C \end{bmatrix}. \tag{37}$$

So the calibration model in this case is

$$\widehat{\mathbf{A}}_{\mathbf{c}}\mathbf{\Gamma} = \mathbf{Q}\mathbf{A}(\theta_c). \tag{38}$$

Then equation (36) can now be changed as

$$[\mathbf{\Gamma}, \widehat{\mathbf{Q}}] = \arg\min_{\mathbf{\Gamma},\mathbf{Q}} \left\| \widehat{\mathbf{A}}_{\mathbf{c}}\mathbf{\Gamma} - \mathbf{Q}\mathbf{A}(\theta_c) \right\|_F^2 , \tag{39}$$

Which means that we estimate both the correction matrix $\mathbf{Q}$ and the unknown gain and phases in $\boldsymbol{\Gamma}$.

To solve this equation, $\boldsymbol{\Gamma}$ is initialized as a unit matrix in the first step, it's expressed by $\boldsymbol{\Gamma_0} = \mathbf{I}$. Then the solution is the same as the global full matrix calibration, so $\widehat{\mathbf{Q}}$ can be computed in the same way. Let k denote the iteration counts of updating $\boldsymbol{\Gamma}$ and $\mathbf{Q}$.

$$\text{k=0}\,, \quad \boldsymbol{\Gamma_0} = \mathbf{I}\ ,\ \widehat{\mathbf{Q}}_0 = \widehat{\mathbf{A}}_\mathbf{c}\mathbf{A}^*(\theta_c)(\mathbf{A}(\theta_c)\mathbf{A}^*(\boldsymbol{\theta_c}) + \lambda\mathbf{I})^{-1}. \tag{40}$$

The next step is to update $\boldsymbol{\Gamma}$ by fixing $\mathbf{Q} = \widehat{\mathbf{Q}}_\mathbf{0}$,

$$\begin{aligned}\text{k=1,}\quad \widehat{\boldsymbol{\Gamma}}_\mathbf{1} &= \arg\min_{\boldsymbol{\Gamma}} \left\|\widehat{\mathbf{A}}_\mathbf{c}\boldsymbol{\Gamma} - \widehat{\mathbf{Q}}_\mathbf{0}\mathbf{A}(\theta_c)\right\|_F^2 \\ &= \arg\min_{\boldsymbol{\Gamma}}(\left\|\hat{\mathbf{a}}_1 r_1 - \widehat{\mathbf{Q}}_0\mathbf{a}(\theta_1)\right\|_F^2 + \cdots + \left\|\hat{\mathbf{a}}_c r_c - \widehat{\mathbf{Q}}_\mathbf{0}\mathbf{a}(\theta_c)\right\|_F^2). \end{aligned} \tag{41}$$

Since $r_1, r_2, \ldots\ldots r_C$ are not related, they can be found independently. Then use this updated $\widehat{\boldsymbol{\Gamma}}_\mathbf{1}$ to compute $\widehat{\mathbf{Q}}_\mathbf{1}$.

$$\text{k=1,}\quad \widehat{\mathbf{Q}}_\mathbf{1} = \widehat{\mathbf{A}}_\mathbf{c}\,\boldsymbol{\Gamma}_\mathbf{1}\mathbf{A}^*(\theta_c)(\mathbf{A}(\theta_c)\mathbf{A}^*(\boldsymbol{\theta_c}) + \lambda\mathbf{I})^{-1}. \tag{42}$$

Determine if $\boldsymbol{\Gamma}$ and $\mathbf{Q}$ has converged or not, by checking if it satisfies some stopping criterion or not. For example

$$\left\|V(\widehat{\boldsymbol{\Gamma}}_{k-1}, \widehat{\mathbf{Q}}_{k-1}) - V(\widehat{\boldsymbol{\Gamma}}_k, \widehat{\mathbf{Q}}_k)\right\| < \varepsilon, \tag{43}$$

where $V(\boldsymbol{\Gamma}, \mathbf{Q}) = \left\|\widehat{\mathbf{A}}_\mathbf{c}\boldsymbol{\Gamma} - \mathbf{Q}\mathbf{A}(\theta_c)\right\|_F^2$. If it does not satisfy this inequality, then update $\boldsymbol{\Gamma}$ and $\mathbf{Q}$ again as in (41) and (42) until the method converges:

$$\widehat{\boldsymbol{\Gamma}}_k = \arg\min_{\boldsymbol{\Gamma}} \left\|\widehat{\mathbf{A}}_\mathbf{c}\boldsymbol{\Gamma} - \widehat{\mathbf{Q}}_{k-1}\mathbf{A}(\theta_c)\right\|_F^2\ , \tag{44}$$

$$\widehat{\mathbf{Q}}_k = \widehat{\mathbf{A}}_\mathbf{c}\,\boldsymbol{\Gamma}_k\mathbf{A}^*(\theta_c)(\mathbf{A}(\theta_c)\mathbf{A}^*(\boldsymbol{\theta_c}) + \lambda\mathbf{I})^{-1}. \tag{45}$$

We implemented this method in MATLAB with a small modification. The gain of the emitting signals should be the same, but the phases are hard to predict if the signal emits continuously while the array rotates. Assume $g_c = 1,\ \ r_c = \exp(j\varphi_c)$. Then we modify (41) to search for the phase only:

$$\varphi_c = \arg\min_{\varphi_c} \left\|\hat{\mathbf{a}}_c\exp(j\varphi_c) - \widehat{\mathbf{Q}}_\mathbf{0}\mathbf{a}(\theta_c)\right\|_F^2\ . \tag{46}$$

Then φ_c can be found by a grid search in MATLAB.

Figure 60 shows the estimated phase versus DOAs. It indicates that the phase of the emitted signal is 360° (or 0°) for DOA = [-60 60] deg. The phase is almost linearly increasing / decreasing near the limits of the incidence angles.

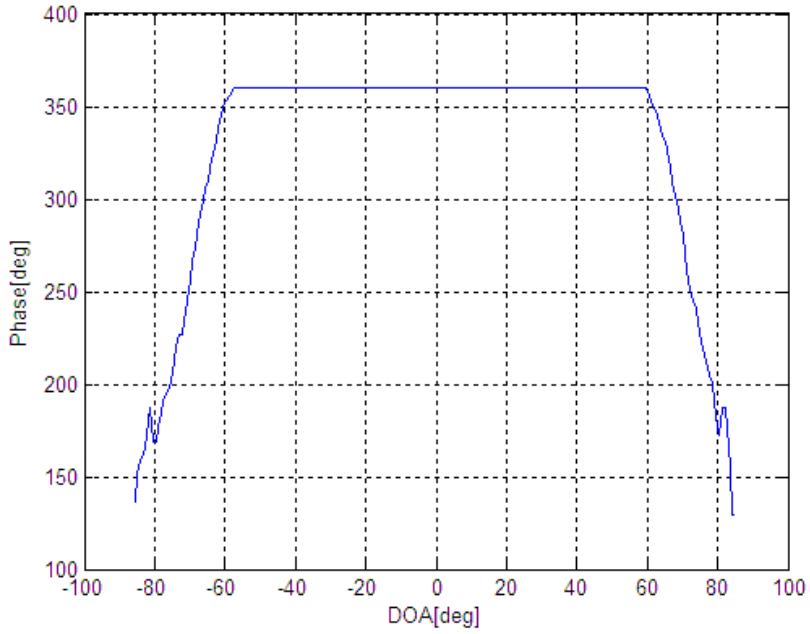

Fig. 60. Estimated phases of emitted signals using dataset 112, f_c = 250 KHz

Figures 61 and 62 show the amplitude and phase of the correction matrix $\widehat{\mathbf{Q}}$. It is similar to the $\widehat{\mathbf{Q}}$ obtained from the global full matrix calibration method, as shown in Figures 21 and 22. Figure 63 plot the diagonal entries of these two calibration matrices, it is now easier to see that this method, calibration with unknown phase, changed the correction matrix a little, especially in the edge.

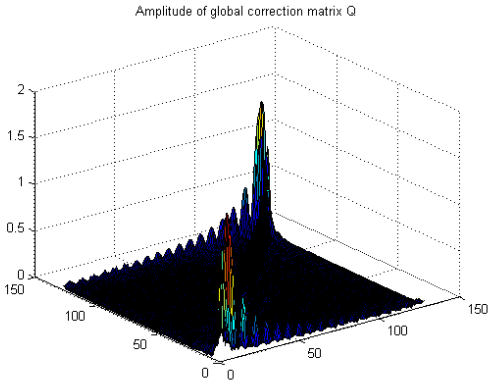

Fig. 61. Calibration with unknown phase
The amplitude of the correction matrix

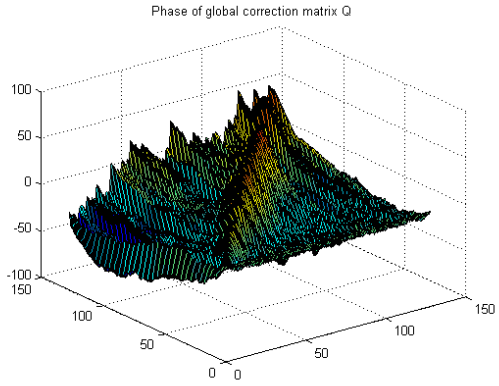

Fig. 62. Calibration with unknown phase
The phase of the correction matrix

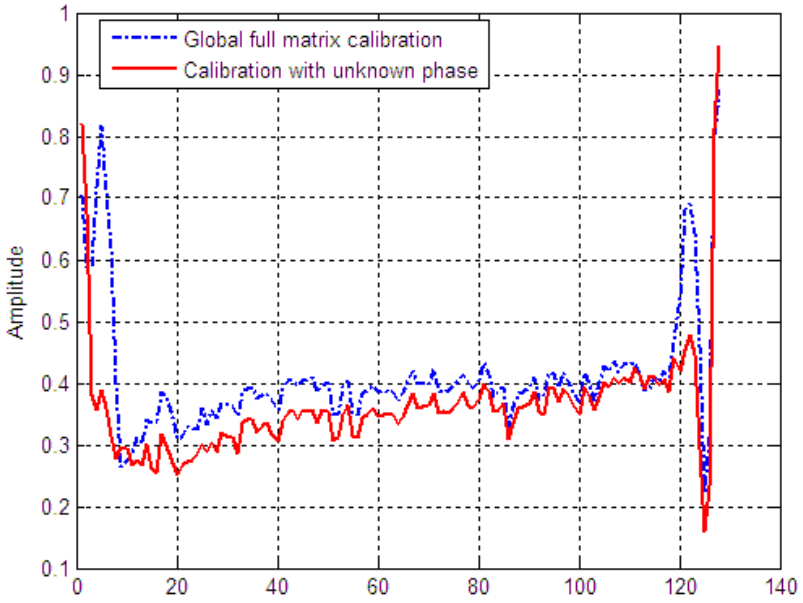

Fig. 63. Diagonal entries of the two correction matrix $\widehat{\mathbf{Q}}$

Table 7 states the DOA RMS errors when using this method and global full matrix calibration. As compared to global full matrix calibration, the calibration method with unknown phase gets better performance when the DOA range is [-80 80] degree, it improves the DOA estimation accuracy around 25%.

Table 7 DOA RMS error Δ

($\widehat{\mathbf{Q}}$ is obtained from data set 112, f_c=250 KHz, $\theta_c = [-80\ 80]$deg)

Δ[deg]	112	124	124_1	124_2	124_3	125
Full Matrix Calibration	0.2347	0.1082	0.1633	0.1679	0.1453	0.2015
Unknown phase calibration	0.0502	0.0701	0.0933	0.0750	0.0707	0.0667
Without calibration	0.0964	0.1664	0.0764	0.0798	0.0782	0.1427

Table 8 shows the DOA RMS errors when setting DOA range as [-70 70] degree. The two calibration methods have similar performance. Both of them improve the accuracy around 50%.

Table 8 DOA RMS error Δ

($\widehat{\mathbf{Q}}$ is obtained from data set 112, f_c=250 KHz, $\theta_c = [-70\ 70]$deg)

Δ[deg]	112	124	124_1	124_2	124_3	125
Full Matrix Calibration	0.0439	0.0498	0.0672	0.0552	0.0479	0.0478
Unknown phase calibration	0.0330	0.0509	0.0552	0.0446	0.0432	0.0457
Without calibration	0.0934	0.1352	0.0717	0.0784	0.0770	0.1178

In Table 9, the DOA RMS error is computed with different f_c. It shows that the calibration method with unknown phase has a better performance than the global full matrix calibration. Still, for higher frequencies the performance is not much better than using no calibration.

Table 9 DOA RMS error Δ

($\widehat{\mathbf{Q}}$ is obtained from dataset 112, $\mathbf{x}[n]$ is obtained from dataset 124, $\theta_c = [-80\ 80]$deg)

Frequency	200 KHz	300 KHz	350 KHz	400KHz
Full Matrix Calibration	0.0817 deg	0.1293 deg	0.1844 deg	0.1740 deg
Unknown Phase Calibration	0.0823 deg	0.0685 deg	0.1426 deg	0.1440 deg
Without Calibration	0.1820 deg	0.1456 deg	0.1436 deg	0.1561 deg

Chapter 7 Conclusions

In this thesis, we tried different approaches for global and local calibration on the specified uniform linear array. Algorithms to estimate the array response vectors and strategies to use it in beamforming algorithms were discussed. Their performances are discussed in Section 5.5, and it can be summarized as follows:

1) The global diagonal matrix calibration is unable to improve the beamforming performance of this array, since it can only compensate for channel errors. But except channel errors, mutual coupling and DOA-dependent errors also exist in this system.
2) Except channel errors, the global full matrix calibration works on the mutual coupling as well. It achieves 50% improvement on DOA estimation accuracy for DOA range [-70 70] degree, but it doesn't work when the DOA range is enlarged to [-80 80] degree. This can be concluded as this method has difficulties to correct model errors near the limits of the useful DOA range.
3) Local calibration shows its superior performance compared to the global calibration methods. The corrected steering vector is almost collinear to the true steering vector, and it provides high improvement on the accuracy of DOA estimation. Unlike global calibration, local calibration deals with general errors including DOA-dependent errors, so it works well for all the frequencies with DOA range [-80 80] degree. The performances are improved 34% and 53% for DOA range [-80 80] and [-70 70] degree separately. But local calibration method needs more computational effort and higher memory requirement.

In the experiment to estimate array response for different f_c ranging from 200 KHz to 400 KHz, the frequency dependency of the array response can be observed. The array response is varying in both amplitude and phase, which means that the array response is frequency dependent. And it's impossible to obtain a constant calibration matrix that can be used on different frequencies. To some extent, the full calibration matrix can be regarded as a mutual coupling matrix, it is also shown in Section 5.5.

Calibration with unknown phase and gain is introduced in the end. It has a similar performance as global full matrix calibration when the DOA range is [-70 70] degree (50% improvement).. And it improves the performance for DOA range [-80 80] degree as well (25% improvement). The estimated phase also explained why the global full matrix calibration method is unable to work near the edge of the useful DOA range.

References

[1] M. Viberg, M. Lanne, A. Lundgren, ''Calibration in Array Processing'', chapter 3 in the book *Classical and Modern Direction-of-Arrival Estimation*, T. Engin Tuncer, B. Friedlander (Editors), Academic Press, July 2009, pp. 93-121.

[2] A. L. Swindlehurst, "Robust Algorithm for Direction Finding in the Presence of Model Errors", *Proc. 5th ASSP Workshop on Spectrum Estimation and Modelling.* Rochester, New York, Oct 1990.

[3] M. Schoor and B. Yang, '' Local and Global Calibration for High-Resolution DOA Estimation in Automotive Radar'', *Sensor Array and Multichannel Signal Processing Workshop*, 2008.

[4] T. Dang, B. Wu, F. Meng, ''A Constrained Algorithm for Gain/Phase and Mutual Coupling Errors Calibration of ULA'', *Asia-Pacific Youth Conference on Communication Technology*, 2010.

[5] L. Gupta, R. P. Singh, ''Array Signal Processing: DOA Estimation for Missing Sensors'', *World Academy of Science*, 2011.

[6] H. Krim and M. Viberg,''Two Decades of Array Signal Processing Research'', *IEEE signal Processing Magazine*, July 1996.

[7] M. Lanne, M. Viberg, A. Lindgren, ''Adaptive beamforming using calibration vectors with unknown gain and phase'', *Antennas and Propagation Society International Symposium,* 2007.

[8] A. Neumaier, "Solving ill-conditioned and singular linear systems: A tutorial on regularization", *SIAM Review 40*, 1998, pp. 636-666.